

Retrotransposon derepression leads to activation of the unfolded protein response and apoptosis in pro-B cells

Alessandra Pasquarella¹, Anja Ebert^{2*}, Gustavo Pereira de Almeida^{1*}, Maria Hinterberger³, Maryam Kazerani¹, Alexander Nuber¹, Joachim Ellwart⁴, Ludger Klein³, Meinrad Busslinger² and Gunnar Schotta^{1§}

¹Ludwig Maximilians University and Munich Center for Integrated Protein Science (CiPS^M), Biomedical Center, Planegg-Martinsried, Germany

²Research Institute of Molecular Pathology, Vienna Biocenter, Vienna, Austria

³Ludwig Maximilians University, Institute for Immunology, Munich, Germany

⁴Helmholtz Zentrum München, Institute of Molecular Immunology, Munich, Germany

*these authors contributed equally

§To whom correspondence should be addressed:

LMU Munich, Biomedical Center, Grosshaderner Strasse 9, 82152 Planegg-Martinsried

phone: +49-89-2180 75 422

fax: +49-89-2180 75 425

e-mail: gunnar.schotta@med.uni-muenchen.de

Abstract

The H3K9me3-specific histone methyltransferase Setdb1 impacts on transcriptional regulation by repressing both developmental genes and retrotransposons. How impaired retrotransposon silencing may lead to developmental phenotypes is currently unclear. Here we show that loss of Setdb1 in pro-B cells completely abrogates B cell development. In pro-B cells, Setdb1 is dispensable for silencing of lineage-inappropriate developmental genes. Instead, we detect strong derepression of endogenous Murine Leukemia Virus (MLV) copies. This activation coincides with an unusual change in chromatin structure with only partial loss of H3K9me3 and unchanged DNA methylation, but strongly increased H3K4me3. Production of MLV proteins leads to activation of the unfolded protein response pathway and apoptosis. Thus, our data demonstrate that B cell development critically depends on the proper repression of retrotransposon sequences through Setdb1.

Epigenetic mechanisms regulate developmental transitions by mediating activation or stable repression of lineage-appropriate or lineage inappropriate genes, respectively. Dysregulation of epigenetic machineries has therefore adverse consequences for development. In the context of hematopoiesis, impairment of repressive chromatin marks, such as DNA methylation or Polycomb silencing, result in compromised stem and progenitor cell differentiation and may even lead to the development of malignancies (Beguelin et al., 2013; Su et al., 2003). Another major repression mechanism involves the heterochromatin modification H3K9me3. This modification is broadly enriched at pericentric heterochromatin, various classes of retrotransposons, imprinted loci and repressed developmental genes. The histone methyltransferase *Setdb1* mainly controls H3K9me3 outside of pericentric heterochromatin and plays crucial roles for development (Karimi et al., 2011; Regha et al., 2007). *Setdb1* mutant embryos die even before implantation (Dodge et al., 2004) and conditional inactivation of *Setdb1* during neurogenesis or in mesenchymal cells coincides with severe developmental phenotypes (Lawson et al., 2013; Tan et al., 2012; Yang et al., 2013). Thus, *Setdb1*-mediated H3K9me3 appears to critically regulate developmental transitions.

The functions of *Setdb1* have been well characterized in mouse embryonic stem (ES) cells. In these cells, *Setdb1* depletion leads to derepression of lineage-specifying genes and loss of pluripotency. Transcriptional dysregulation in *Setdb1*-deficient ES cells is due to the loss of H3K9me3 from promoter regions of lineage genes (Bilodeau et al., 2009; Yuan et al., 2009). In addition, *Setdb1*-deficient ES cells are characterized by enhanced transcription of retrotransposons. To what extent retrotransposon derepression may lead to phenotypic consequences is unclear. Two hypotheses are currently discussed: 1) Derepression of retrotransposons leads to elevated transcription of neighboring genes through enhancer action of chimeric transcripts (Karimi et al., 2011; Matsui et al., 2010). This, in turn, may impair the transcriptional stability in cells. 2) Enhanced activity of functional retrotransposon copies which are still able to jump may lead to mutations (Lee et al., 2012) or genomic instability (Bourc'his and Bestor, 2004).

Here we show that conditional inactivation of *Setdb1* in pro-B cells leads to a block in B cell development. We found that *Setdb1*-deficient pro-B cells show derepression of specific classes of retrotransposons, among which the endogenous murine leukemia virus (MLV) elements exhibited the highest transcriptional activation. Notably, forced MLV expression coincides with massive production of MLV-derived proteins which, in turn, triggers activation of the unfolded protein response (UPR) and subsequent apoptosis of pro-B cells. Expression of pro-survival *Bcl-2* antagonizes UPR-mediated apoptosis and leads to a partial rescue of B

cell development, indicating that retrotransposon silencing is the primary role of *Setdb1* during early B cell development. In summary, our data provide a novel molecular explanation for the adverse consequences of impaired retrotransposon silencing during development.

Results

Loss of *Setdb1* blocks B cell development

Setdb1 is constitutively expressed during B cell development (Heng et al., 2008). To delete *Setdb1* specifically during early stages of B cell development we generated a mouse strain where we combined a conditional *Setdb1* allele with the critical exon 4 flanked by loxP sites with *Mb1-Cre* (*Cd79a-Cre*) mice (*Mb1-Cre; Setdb1^{lox/delta}* mice, further denoted as *Setdb1^{Mb1}* and *Mb1-Cre; Setdb1^{lox/+}* or *+/+; Setdb1^{lox/+}* further denoted as *control*). *Mb1-Cre* initiates deletion of loxP flanked regions at the transition from pre-pro-B cells to committed pro-B cells (Hobeika et al., 2006). Spleen size was severely reduced in *Setdb1^{Mb1}* mice (Figure 1A). Histological examination revealed reduced number and size of follicles (Figure 1B). The total cell numbers of spleen and bone marrow were strongly reduced in *Setdb1^{Mb1}* mice (Figure 1C). Consistent with the lack of *Mb1-Cre* activity in T cell development, no changes in thymus cell numbers were detected (Figure 1C). FACS analysis of B cell markers revealed almost complete absence of B cells (B220⁺ CD19⁺) in *Setdb1^{Mb1}* spleen and severely reduced B cell numbers in bone marrow (Figure 1D,E). The lack of peripheral B cells prompted us to identify the stage at which B cell development is impaired in *Setdb1^{Mb1}* mice. Analysis of the B cell compartment in bone marrow revealed that percentages of pro-B cells (CD19⁺ IgM⁻ IgD⁻ CD25⁻ Kit⁺) are comparable between *control* and *Setdb1^{Mb1}* mice, however, pre-B cells (CD19⁺ IgM⁻ IgD⁻ CD25⁺ Kit⁻) were severely reduced and neither immature (B220⁺ IgM⁺ IgD⁻) nor recirculating B cells (B220⁺ IgM⁻ IgD⁺) could be detected (Figure 1F,G). Analysis of hematopoietic stem cell and progenitor populations revealed no difference between *control* and *Setdb1^{Mb1}* mice, as expected (Supplementary Figure 1).

To test if blocked B cell development was due to cell intrinsic defects we performed competitive transplantation experiments by injecting a 1:1 mixture of wild type CD45.1 bone marrow progenitors together with *control* or *Setdb1^{Mb1}* bone marrow cells carrying the congenic marker CD45.2 into lethally irradiated recipients. Whereas the *control* bone marrow cells contributed to the B cell lineage comparably to the co-injected wild type cells, *Setdb1^{Mb1}* B cells were hardly detectable in the periphery (Figure 2A). Analysis of the B cell compartment in the bone marrow of transplanted mice revealed that *Setdb1^{Mb1}* B cells were

severely compromised at the pre-B cell stage (Supplementary Figure 2).

We then performed *in vitro* B cell differentiation assays. Control bone marrow cells readily formed colonies in IL-7 supplemented MethoCult M3630 medium which supports B cell differentiation. Conversely, almost no colonies were obtained from *Setdb1*^{Mb1} bone marrow (Figure 2B). Further, *in vitro* differentiation of lineage-depleted bone marrow cells on OP9 stromal cells in the presence of IL-7 revealed severely impaired differentiation of *Setdb1*^{Mb1} progenitors into the B cell lineage (Figure 2C). Thus our data demonstrate an essential cell autonomous function of Setdb1 in early stages of B cell development.

Transcriptional changes in *Setdb1*^{Mb1} pro-B cells

To identify the molecular mechanisms leading to impaired B cell development in the absence of Setdb1 we performed transcriptional profiling by high-throughput RNA sequencing (RNA-seq). RNA was isolated from FACS sorted pro-B cells (CD19⁺ IgM⁻ IgD⁻ CD25⁻ Kit⁺) from *control* and *Setdb1*^{Mb1} mice. Setdb1 was completely deleted in *Setdb1*^{Mb1} pro-B cells as no band could be detected upon PCR amplification of the floxed exon 4 (Figure 3B). Through RNA-seq analysis we found 130 up- and 136 down-regulated (>2 fold) genes in *Setdb1*^{Mb1} pro-B cells (Figure 3A, Supplementary Table 1). GO term analysis of the regulated genes revealed enrichment for pathways implicated in immune system development (Figure 3C). However, closer examination of the dataset pointed out that none of the known essential factors for B cell development were dysregulated. Rather we found transcriptional changes of genes which are normally regulated during pro-B to pre-B cell transition. One example is *Aiolos* (*Ikzf3*) which is normally upregulated in late pro-B cells. *Aiolos* expression was detected in *control* pro-B cells, but it failed to be activated in *Setdb1*^{Mb1} pro-B cells. This suggested that the pro-B cell population isolated from *Setdb1*^{Mb1} bone marrow resided in a more immature stage. To further substantiate this finding we performed gene set enrichment analysis using gene sets which are representative of early pro B and late pro-B/early pre-B cells, respectively (Jojic et al., 2013). Notably, the early pro-B signature was enriched in *Setdb1*^{Mb1} pro-B cells, whereas the late pro-B/early pre-B signature was overrepresented in *control* cells (Figure 3D). These analyses suggest a bias toward having reduced numbers of late pro-B/early pre-B cells in *Setdb1*^{Mb1} bone marrow. In order to test this hypothesis we analyzed B cell populations using a different marker set (Hardy et al., 1991). We found significantly reduced late pro-B/early pre-B cells (B220⁺ CD43⁺ HSA⁺ BP1^{+/-}) in *Setdb1*^{Mb1} mice (Supplementary Figure 3). These data suggest that the majority of the transcriptional

changes that we detected by RNA-seq simply reflect the block in pro-B to pre-B cell transition in *Setdb1*^{Mb1} mice.

Setdb1 directly regulates retrotransposons

To identify genomic regions which may be controlled by Setdb1 in pro-B cells we performed chromatin immunoprecipitation for Setdb1, H3K9me3 and H3K9ac in short-term cultured *Rag2*^{-/-} pro-B cells followed by high throughput sequencing (ChIP-seq). This analysis revealed 5368 Setdb1 binding sites in pro-B cells, which are shared in two independent datasets (see Supplementary Figure 4 for analysis of the individual datasets). To determine at which binding sites Setdb1 could induce H3K9me3 we calculated the ChIP-seq read coverage for Setdb1, H3K9me3 and H3K9ac in 1500 bp windows across all Setdb1 binding sites. These data were then clustered according to H3K9me3 and H3K9ac density (Figure 4A). This analysis revealed that only a subset of Setdb1 binding sites associates with H3K9me3 (clusters A,B). A large number of Setdb1 peaks is found together with H3K9ac (clusters D,E,F) or does not display prominent enrichment for either H3K9me3 or H3K9ac (clusters C,G). We then analyzed the structural features underlying Setdb1 binding sites. H3K9me3-associated regions are clearly enriched for repeat elements (clusters A,B). In contrast, H3K9ac-rich Setdb1 peaks are mainly present at promoter regions (clusters D,E,F). We then asked if genes nearby Setdb1 binding sites are transcriptionally regulated in *Setdb1*^{Mb1} pro-B cells. For each cluster, genes with a transcriptional start site in 5 kb proximity to the Setdb1 binding site were extracted. However, we could not detect significant enrichment of regulated genes in any of the Setdb1 binding site clusters. These data demonstrate that in pro-B cells Setdb1 regulates only a small number of genes in the vicinity of its binding sites.

The ChIP-seq analysis showed that Setdb1 binding sites which are enriched for H3K9me3 (clusters A,B) mainly reside within repeat elements. Therefore we investigated whether distinct classes of repeat elements are dysregulated in *Setdb1*^{Mb1} pro-B cells. Analysis of our RNA-seq data uncovered three classes of retrotransposons (MLV, MMVL30 and MMTV) to be upregulated in *Setdb1*^{Mb1} pro-B cells (Supplementary Table 2, Supplementary Figure 5A). Re-examination of RNA-seq reads with unique mapping in the genome allowed to distinguish individual copies of these retrotransposons classes. The most strongly upregulated retrotransposons were four copies of the MLV class with >100 fold over-expression (Figure 4B). Notably, these four copies showed the strongest enrichment for Setdb1 and H3K9me3 (Figure 4C). Intriguingly, major targets of Setdb1 in embryonic stem cells, IAP-Ez

retrotransposons, were also enriched for Setdb1 and H3K9me3 in pro-B cells, but did not show significantly enhanced expression in *Setdb1*^{Mbl} pro-B cells (Figure 4B,C).

In summary, our data suggest that although Setdb1 occupies many binding sites in pro-B cells, only a subset of these regions correlates with changes in gene expression when Setdb1 is absent. Our results show that in pro-B cells the major repressive function of Setdb1 is exerted on specific classes of retrotransposons.

Setdb1 mediates MLV silencing in pro-B cells

Our ChIP-seq data revealed strongest enrichment of Setdb1 and H3K9me3 at distinct MLV elements. Close inspection of the genomic regions around the derepressed MLV retrotransposons revealed that genes in close proximity were also highly upregulated. An example is the MLV retrotransposon on chromosome 8 in vicinity of *Tubb3* and *Def8* (MLV8, Figure 5A). *Tubb3* encodes a neuron-specific tubulin involved in axon guidance; *Def8* (differentially expressed in FDCP 8) is a largely uncharacterized gene of unknown function. RNA-seq data show strong derepression of MLV8 and upregulation of both *Tubb3* and *Def8*. Notably, upregulation of both genes is not mediated by read-through transcripts originating from MLV8 which is oriented tail-to-tail with *Tubb3* and head-to-head with *Def8*. ChIP-seq data revealed enrichment of Setdb1 and H3K9me3 across MLV8, but only background levels were detected across *Tubb3* and *Def8*. These data suggest that loss of Setdb1 leads to derepression of MLV8 which then exerts enhancer effects on the neighboring genes leading to their upregulation. A similar example is MLV1 which is in proximity to the *Fcgr2b* gene (Supplementary Figure 5B). In *Setdb1*^{Mbl} pro-B cells, both MLV1 and *Fcgr2b* are strongly derepressed (Figure 5B) and *Fcgr2b* protein is even highly incorporated into the cell membrane (Supplementary Figure 5C,D). Interestingly, *Fcgr2b* is also upregulated in *Setdb1*-deficient T cells (Martin et al., 2015), although, it remains to be determined if derepression of MLV1 can be observed in this context. RT-qPCR analyses for another MLV element (MLV5) similarly revealed strong derepression of the corresponding MLV transcript and upregulation of the neighboring gene (Figure 5B).

To test whether Setdb1-dependent chromatin changes lead to dysregulation of MLV elements we isolated *control* and *Setdb1*^{Mbl} CD43⁺, CD19⁺ pro-B cells by FACS sorting and performed ChIP-qPCR analyses. H3K9me3 was prominently enriched on MLV elements; however, loss of Setdb1 did only result in a small reduction of this modification (Figure 5C). It is possible that other HMTases, such as Suv39h, contribute to H3K9me3 establishment (Bulut-Karslioglu

et al., 2014). H3K4me3, a mark of active chromatin, was strongly elevated on MLV elements and on the promoters of *Tubb3* and *Def8* in *Setdb1*-deficient pro-B cells (Figure 5D). No enrichment of H3K4me3 could be detected on IAP-Ez elements, which showed no transcriptional changes in *Setdb1*^{Mb1} pro-B cells. We also tested whether any changes in DNA methylation may contribute to transcriptional activation of these MLV elements. Very high DNA methylation was detected in the strongly upregulated MLV8, demonstrating that loss of DNA methylation is not required for transcriptional activation (Figure 5E, Supplementary Figure 6). IAP elements and a transcriptionally unchanged MLV retrotransposon did not show any changes in DNA methylation (Figure 5E, Supplementary Figure 6). Our data suggest that the presence of *Setdb1* inhibits binding and/or activity of specific transcription factors which otherwise establish an active chromatin structure. Complete loss of H3K9me3 or DNA methylation is apparently not necessary to allow establishment of H3K4me3 and productive transcription.

***Setdb1*^{Mb1} pro-B cells die through apoptosis**

Our transcriptional profiling of *Setdb1*^{Mb1} pro-B cells did not reveal dysregulation of important B cell related transcription factors which could have explained a developmental block. Another explanation for impaired B cell development could be that pro-B cells die from apoptosis. To test if apoptosis is elevated in *Setdb1*^{Mb1} pro-B cells we performed Annexin V staining on *control* and *Setdb1*^{Mb1} bone marrow cells. In *control* mice around 30% of pro-B cells enter apoptosis, likely due to non-productive VDJ recombination. Interestingly, apoptosis rate was strongly increased in *Setdb1*^{Mb1} pro-B cells (Figure 6A).

If enhanced apoptosis of pro-B cells is a major reason why B cell development is blocked in *Setdb1*^{Mb1} mice we would predict that introducing a pro-survival protein may compensate for *Setdb1* deficiency in B cell development. To test this hypothesis we introduced an allele that over-expresses anti-apoptotic *Bcl2* in all hematopoietic cells (*Vav-Bcl2* (Egle et al., 2004)) into *Setdb1*^{Mb1} mice. Apoptosis in both *Bcl2* and *Setdb1*^{Mb1}; *Bcl2* pro-B cells was comparably low (Figure 6B). We then examined B cell development in the bone marrow of *Setdb1*^{Mb1}; *Bcl2* mice. Compared to *Setdb1*^{Mb1} (Figure 1F,G) there was an increase in percentages of pre-B, immature B and mature B cells in *Setdb1*^{Mb1}; *Bcl2* mice (Supplementary Figure 7). Significant numbers of *Setdb1*-deficient mature B cells could be observed in the spleen of *Setdb1*^{Mb1}; *Bcl2* mice (Figure 6C-E), which were virtually absent in *Setdb1*^{Mb1} mice (Figure 1D,E). These results were further supported by *in vitro* differentiation experiments with

lineage-depleted bone marrow cells from *Bcl2* and *Setdb1^{Mbl}*; *Bcl2* mice which showed almost comparable growth of pre-B cell colonies (Figure 6F). An important process during pro-B cell development is V-DJ recombination of the *Igh* locus to produce a functional pre-B cell receptor. Consistent with the block in pro-B to pre-B transition in *Setdb1^{Mbl}* mice, we detected lower efficiency of V-DJ rearrangement (Supplementary Figure 8). In contrast, V-DJ recombination was unaffected in *Setdb1^{Mbl}*; *Bcl2* pro-B cells (Supplementary Figure 8). Thus, our data demonstrate that counteracting apoptosis can partially rescue the developmental phenotype of *Setdb1^{Mbl}* mice.

Activation of the unfolded protein response pathway in *Setdb1^{Mbl}* pro-B cells

We then wondered if apoptosis may be linked with the transcriptional changes that we observe in *Setdb1^{Mbl}* pro-B cells. As we only detected moderate regulation of protein-coding genes (Figure 3), we hypothesized that upregulation of retrotransposons may lead to apoptosis. Upregulation of ERVs has been connected with enhanced DNA damage that may lead to apoptosis. However, we did not detect increased DNA breaks in *Setdb1^{Mbl}* B cells (Supplementary Figure 9). We then tried to understand if transcription of retrotransposons leads to the production of retroviral proteins. The top regulated retrotransposon class in *Setdb1^{Mbl}* pro-B cells is MLV retrotransposons. MLV transcripts have coding potential and can lead to the production of retroviral proteins. For example, the retroviral envelope protein is produced as glycosylated membrane protein and can be detected on cells with elevated expression of MLV transcripts (Evans et al., 1990; Young et al., 2012). We tested MLV env protein production by FACS analysis and could detect high levels on the surface of *Setdb1^{Mbl}* pro-B cells compared to littermate controls (Figure 7A). Western blot analyses confirmed high expression of MLV Env protein in *Setdb1*-deficient pro-B cells (Supplementary Figure 10A).

Could apoptosis in *Setdb1^{Mbl}* pro-B cells be linked with the excessive production of MLV proteins? Unlike e.g. plasma cells which are specialized for the mass production of secreted proteins (Brewer and Hendershot, 2005; Gass et al., 2004), pro-B cells are relatively small cells with a limited capacity to produce such proteins. Strongly elevated translation of proteins into the endoplasmic reticulum may lead to accumulation of improperly folded proteins which triggers a cellular stress pathway, known as unfolded protein response (UPR). Hence, we tested activation of the UPR pathway in *Setdb1^{Mbl}* pro-B cells by expression analysis of key UPR genes.

A hallmark of the UPR response is the accumulation of a specific splice form of the mRNA

encoding the transcription factor *Xbp1* (Calton et al., 2002). Importantly, compared to *control* pro-B cells, we detected an increased level of spliced *Xbp1* (*Xbp1s*) in *Setdb1*-deficient pro-B cells (Figure 7B). Further, we found elevated expression of pro-apoptotic *Bcl2l1* (Figure 7B). Other key UPR genes, such as the chaperones *Hspa5* (Grp78/BiP) and *Pdia6* (Groenendyk et al., 2014; Lee, 2005), were also upregulated in *Setdb1*-deficient pro-B cells (Figure 7B). As elevated apoptosis in *Setdb1^{Mbl}* pro-B cells may prevent accumulation of UPR transcripts, we also tested the UPR pathway in *Setdb1^{Mbl}; Bcl2* pro-B cells. Notably, we detected even stronger upregulation of key UPR genes in *Setdb1^{Mbl}; Bcl2* pro-B cells (Figure 7B). Further, gene set enrichment analysis using the hallmarks gene sets from MySigDB revealed significant enrichment of the UPR gene signature in *Setdb1^{Mbl}* pro-B cells (Figure 7C). Thus, increased expression of UPR components in both *Setdb1^{Mbl}* and *Setdb1^{Mbl}; Bcl2* pro-B cells clearly demonstrate activation of the unfolded protein response pathway.

The key inducer of apoptosis in the context of UPR is *Bcl2l1* (Puthalakath et al., 2007). To test if apoptosis in *Setdb1^{Mbl}* pro-B cells is really mediated through *Bcl2l1* we performed knock-down experiments in *in vitro* B cell differentiation assays. Control cells with scrambled shRNAs could readily form colonies in MethoCult M3630, whereas *Setdb1^{Mbl}* cells did not form colonies (Figure 7D). Knock-down of *Bcl2l1* in *Setdb1^{Mbl}* cells resulted in significantly elevated colony numbers (Figure 7D), demonstrating that *Bcl2l1* is mainly responsible for apoptosis induction in *Setdb1^{Mbl}* cells.

Finally, we asked whether UPR-mediated apoptosis is mainly caused by over-expression of MLV proteins. We performed *in vitro* differentiation assays of wild type cells in which we over-expressed GFP or MLV Env protein of the endogenous MLV1 retrovirus. Wild type CD19⁺ B cells in which we did not over-express additional proteins show a low rate of apoptosis (Figure 7E). GFP over-expression in B cells did not reveal elevated apoptosis (Figure 7E, Supplementary Figure 10B). In contrast, over-expression of MLV Env protein leads to strongly increased apoptosis in B cells (Figure 7E, Supplementary Figure 10B). Importantly, qRT-PCR analyses of *in vitro* differentiated B cells revealed specific activation of UPR genes upon Env over-expression (Figure 7F).

In summary, our data show that elevated expression of MLV transcripts leads to excessive production of MLV env protein which triggers the UPR pathway leading to apoptosis in *Setdb1^{Mbl}* pro-B cells, resulting in a block of B cell development.

Discussion

Our study demonstrates the crucial requirement to silence specific retrotransposons during development (Figure 7G), which is in full agreement with a recent study of Setdb1 function in B cells (Collins et al., 2015). In wild type cells, Setdb1 binds to MLV retrotransposons and establishes a repressive chromatin structure which prevents access by activating transcription factors. Upon deletion of *Setdb1* in pro-B cells some “responsive” MLV elements display strong transcriptional activity. It is possible that due to the loss of Setdb1, transcription factors can now access these MLVs leading to establishment of active H3K4me3. Interestingly, this activation can occur, although H3K9me3 is only minimally reduced and DNA methylation is unchanged. The activation of MLVs leads to two outcomes. Firstly, responsive MLV retrotransposons may act as enhancers to strongly stimulate the transcription of neighboring genes. Secondly, excessive production of MLV-derived proteins triggers an unfolded protein response in pro-B cells, leading to apoptosis.

Genome-wide Setdb1 binding was so far only characterized in ES cells, where targets include retrotransposons and promoters of developmental genes (Bilodeau et al., 2009; Yuan et al., 2009). In pro-B cells, we also detected Setdb1 on promoter regions, however, we did not observe strong transcriptional changes of these target genes in *Setdb1*-deficient pro-B cells. Interestingly, in pro-B cells, Setdb1 is mostly unable to induce repressive H3K9me3 on promoter binding sites as we detected strong H3K9ac occupancy on these regions. Transcription of these targets does not seem to be affected by Setdb1 loss and, therefore, it is currently unclear which function Setdb1 exerts on such binding sites. The major target sites at which Setdb1 mediates establishment of H3K9me3 and transcriptional repression in pro-B cells are retrotransposons (Figure 4). How Setdb1 is recruited to these elements remains to be clarified. In ES cells targeting is mainly mediated by Trim28, however, Trim28 is not enriched on MLV retrotransposons in B cells (Santoni de Sio et al., 2012). Moreover, Trim28 deletion in the B cell lineage did not result in impaired B cell development, but rather to transcriptional dysregulation in mature B cells (Santoni de Sio et al., 2012). Thus, Trim28-dependent mechanisms are unlikely to mediate Setdb1 targeting to MLVs.

Derepression of retrotransposons in *Setdb1*^{Mbl} pro-B cells implies that absence of Setdb1 allows binding of specific transcription factors to these elements. There is emerging evidence that transposable elements contain transcription factor binding sites (Xie et al., 2010) and may

even physiologically act as tissue-specific enhancers (Xie et al., 2013). A recent study showed that the master B cell transcription factor Pax5 may mediate forced expression of the same MLV elements that we found upregulated in *Setdb1*-deficient pro-B cells (Collins et al., 2015 and Supplementary Table 3). However, additional cell type-specific transcription factors are likely to contribute to MLV transcription, as *Setdb1*-deficient mouse embryonic fibroblasts (Matsui et al., 2010) or myeloid cells (data not shown), which do not express Pax5, also display derepression of MLV retrotransposons. It is interesting to note that in pro-B cells only very few retrotransposon classes are derepressed, whereas *Setdb1*-deficient ES cells show strong derepression of many retrotransposon classes, including IAP-Ez, ETn, MusD and others (Karimi et al., 2011). In particular, in ES cells, the major *Setdb1* targets are IAP-Ez elements which, although bound by *Setdb1* and enriched for H3K9me3, display no transcriptional changes in *Setdb1*^{Mbl} pro-B cells. This may be explained by the lack of IAP-specific transcription factors in pro-B cells. Alternatively, redundant repression mechanisms, such as DNA methylation, may ensure silencing of those repeats in absence of *Setdb1*. Consistent with this hypothesis, we did not detect significant changes in DNA methylation at these elements (Figure 5).

Our data demonstrate that transcripts from endogenous MLV retroviruses have coding potential and lead to the strong production of MLV proteins. In pro-B cells, this triggers activation of the unfolded protein response pathway, and cells enter apoptosis. To our knowledge, this is the first demonstration that retrotransposon activation is linked with this specific cellular stress pathway. Several lines of evidence support our notion that UPR-mediated apoptosis is a major cause of impaired B cell development in *Setdb1*^{Mbl} mice:

- 1.) No critical B cell transcription factors are dysregulated in *Setdb1*^{Mbl} pro-B cells (Figure 3, Supplementary Table 1). The only hematopoiesis-related gene which shows strong upregulation is *Fcgr2b* (Supplementary Figure 5). However, over-expression of *Fcgr2b* does not lead to defective B cell development (Brownlie et al., 2008).
- 2.) The apoptosis phenotype is mainly due to elevated MLV protein expression as over-expression of MLV Env protein is sufficient to induce apoptosis in B cells (Figure 6D). Interestingly, expression of MLV Env protein from exogenous MLV retroviruses also results in increased apoptosis (Zhao and Yoshimura, 2008) and infection with MLV retroviruses results in impaired B cell development *in vivo* (Finstad et al., 2007). Furthermore, it is possible that transcripts/proteins produced from other upregulated repeat elements contribute to the phenotype.

3.) Blocking apoptotic pathways in *Setdb1^{Mbl}*; *Bcl2* mice resulted in a partial rescue of B cell development. Importantly, detection of mature B cells in the spleen of *Setdb1^{Mbl}*; *Bcl2* mice demonstrates that expression of key developmental genes is unlikely to be affected by *Setdb1*. The rescue may be partial because preventing apoptosis by Bcl-2 expression does not cease MLV env production in *Setdb1^{Mbl}*; *Bcl2* pro-B cells. Therefore, those B cells are still compromised and may die through apoptosis-independent pathways.

4.) Apoptosis is mainly due to activation of the UPR pathway. We detect upregulation of key UPR genes in both *Setdb1^{Mbl}* and *Setdb1^{Mbl}*; *Bcl2* pro-B cells (Figure 6B). Knock-down of the key UPR apoptosis inducer *Bcl2l1* leads to rescue in B cell development (Fig. 6C). We also attempted rescue experiments by knocking down other UPR components. However, due to the redundancy in UPR signaling pathways knock-down of individual UPR genes does not compromise UPR activation (Puthalakath et al., 2007). Furthermore, important UPR genes are essential for B cell development (Zhang et al., 2005) and cannot be knocked down. We cannot fully exclude additional causes for apoptosis, such as DNA damage or large-scale changes in chromatin architecture. However, as over-expression of MLV Env protein is already sufficient to induce apoptosis (Figure 6D) and to trigger UPR (Zhao and Yoshimura, 2008) our data strongly suggest that UPR activation is a major cause for apoptosis in *Setdb1^{Mbl}* pro-B cells. Unfortunately, due to the limited number of pro-B cells and the unavailability of good antibodies, protein expression levels of UPR-related genes and protein-protein interactions between MLV derived and UPR proteins could not be further assessed.

UPR-mediated cell death mediated by retrotransposons may not be limited to pro-B cells. Derepression of other retrotransposon classes in different cell types may involve similar mechanisms. For example, apoptosis in *Setdb1*-deficient ES cells (Matsui et al., 2010) or neurons (Tan et al., 2012), which involve strong derepression of IAP retrotransposons may be linked with UPR stress. However, additional cellular stress pathways exist that may detect over-expression of endogenous retroviruses in other systems. For example, production of double stranded RNA from ERVs could be recognized by specific pattern recognition receptors leading to activation of the interferon response pathway (Roulois et al., 2015). Future experiments will reveal which cell types are particularly sensitive to over-expression of ERVs and which cellular pathway(s) can be triggered by distinct ERV classes.

Materials and Methods

Mice and cell lines

Mice carrying the floxed *Setdb1* allele were purchased from the EUCOMM project (*Setdb1^{tm1a(EUCOMM)Wtsi}*). *Mbl-Cre* and *Vav-Bcl2* transgenes have been previously described (Egle et al., 2004; Hobeika et al., 2006). Animals were housed in ventilated cages in the mouse facility at the Adolf Butenandt Institute, in agreement with EU regulations. For the experiments, 5 to 10 weeks old animals were used.

293T, OP9 stroma cells and progenitor cells were cultivated in DMEM (Gibco), IMDM and RPMI (Gibco), respectively. Media were supplemented with 10% FCS, 1% non-essential amino acids, 1% penicillin/streptomycin and 0.2% β -mercaptoethanol (Sigma). For progenitor cell short-term culture RPMI was supplemented with IL-7 (PeproTech).

Flow cytometry and cell sorting

Single cell suspensions from bone marrow and spleen were stained for 20 min at 4°C using combinations of antibodies (see supplementary material and methods) conjugated with fluorochromes detectable in the following channels: FITC, PE, PE-Cy5, Pe-Cy7, APC, APC-Cy7. All samples were pre-incubated for 20 min at 4°C with unconjugated CD16/CD32 Fc-blocking antibody to avoid unspecific binding, unless otherwise indicated. Data were acquired using FACS Canto and cell sorting was performed using either MoFlo or FACS Aria III. Sorted samples were pre-treated with red blood cell lysis buffer (BD Bioscience) or enriched using CD45R (B220) microbeads (Miltenyi). Data from flow cytometry were analyzed using FlowJo software (TreeStar).

Red blood cell lysis

Erythrocyte lysis was performed using BD Pharm Lyse™ purchased from BD Pharmingen. 10x RBC buffer was diluted using distilled water kept at room temperature. 3 ml of 1x RBC lysis buffer were used to treat bone marrow cells derived from one mouse. Bone marrow cells were washed with 1x PBS and centrifuged at RT for 10 min at 1300 rpm. Pellets were incubated for 15 min at RT with appropriate amount of lysis buffer and then centrifuged at RT

for 10 min at 1300 rpm. Cell pellets were then washed with 1x PBS to remove traces of lysis buffer and broken erythrocytes.

Definition of hematopoietic cell types for FACS analysis and FACS sorting

Hematopoietic cell types were defined according to specific surface markers (see supplementary material and methods for details).

Bone marrow transplantation

Bone marrow cells were harvested from CD45.1 wild type and CD45.2 donor mice 3-4 days after 5-FU injection. To perform competitive bone marrow transplantation, 1×10^6 cells from CD45.1 wild type mice were mixed 1:1 with either *control* (+/+; Mb1-Cre) or *Setdb1^{fllox/-}; Mb1-Cre* (*Setdb1^{Mb1}*) mice. The mixture was transplanted into lethally irradiated (9 Gy) wild type mice through tail vein injection. CD45.1 and CD45.2 surface markers were used to discriminate between the donors. Bone marrow and spleen from recipients were analyzed by flow cytometry 7 to 9 weeks after transplantation.

Histological analysis

Spleen from 6-8 weeks old animals were fixed overnight in 4% formaldehyde and embedded in paraffin. Spleen sections were then stained with heamatoxylin/eosin.

B cell colony forming assay and B cell differentiation on OP9 cells

To test B cell differentiation, lineage depleted or whole bone marrow cells were treated with red blood cell lysis buffer were seeded (1×10^5 cells/ml) in duplicate in 60 mm dishes on MethoCult 3630 (Stem Cell Technology) containing IL-7 according to the manufacturer's protocol. Cells were grown at 37°C/5% CO₂ and checked every each day to monitor colony formation. After 10-12 day of culture colonies were scored and subsequently analyzed by flow cytometry using B220 and CD19 markers in combination with the viability dye 7AAD. For short-term culture of B cell progenitors, lineage negative bone marrow cells were enriched via magnetic sorting using the lineage cell depletion kit (Miltenyi). 5×10^5 to 1×10^6 cells were seeded in 24 well plates together with OP9 stromal cell in the presence of IL-7 (10

ng/ml). Every other day cells were split onto a fresh OP9 cell layer with IL-7 supplemented medium as previously described (Holmes and Zuniga-Pflucker, 2009). At day 10 of co-culture cells were harvested and analyzed by flow cytometry for pre-B cell differentiation using the Hardy scheme (Hardy et al., 1991).

Annexin V staining

Annexin V staining was performed using Annexin V apoptosis detection kit (ebioscience). 1-2 x10⁶ bone marrow cells were pre-stained with pro-B cell markers. Next, cells were washed once with PBS and then with 1 ml of 1x Annexin V buffer. Pellets were resuspended in 100 µl of Annexin V buffer to which 5 µl of Annexin V were added. Cells were incubated in the dark at RT for 15 minutes. To remove unbound Annexin V cells were washed with 1-2 ml of Annexin V buffer and immediately analysed by FACS.

Expression analysis by qRT-PCR

Pro-B cells were sorted either with MoFlo or FACS Aria. For gene expression analyses in *Setdb1*^{Mbl} pro-B cells, RNA was isolated using the RNeasyPlus kit (Qiagen). Genomic DNA retained by the gDNA columns was purified and used to test the deletion rate.

Alternatively, to detect gene expression changes in *Setdb1*^{Mbl}; *Bcl2* pro-B cells, mRNA was isolated using TRIZOL or Direct-zol RNA MiniPrep (Zymo research). To remove genomic DNA contaminations, samples were treated with DnaseI (Roche). cDNA was synthesized using random hexamer primers. Ct values were obtained by performing qPCR using the SYBR green dye. Differences in gene expression were calculated either as fold change using the 2-ΔΔCT algorithm or as relative expression to housekeeping genes.

RNA-Seq

Pro-B cells were sorted using MoFlo and RNA was isolated using the RNeasyPlus kit (Qiagen). Library preparation was performed as in (Schwickert et al., 2014).

ChIPseq and ChIP-qPCR

Short-term cultured Rag2^{-/-} pro-B cells were obtained in vitro by cultivating them together with OP9 stromal cells in the presence of IL-7. After 5-6 days of expansion CD19⁺ B cells were enriched by magnetic sorting and processed to precipitate chromatin using the following antibodies: α -Setdb1, α -H3K9me3, α -H3K9ac according to (Schwickert et al., 2014).

Statistical analysis

Statistical differences between control and mutant groups were determined by unpaired or paired t-tests. P values of <0.05 were considered significant. Graphs and statistical tests were done using R. Bargraphs shows mean values; error bars denote standard deviation.

shRNA knock-down and MLV overexpression in B cells

The coding sequence of the envelope protein encoded by MLV1 was PCR-amplified using the following primer pair: 5'-ATGGAAGGTCCAGCGTTCT-3' and 5'-ACCAAGAACAAACCCAGCT-3'. The amplicon was gel-purified and used as template for a second amplification performed with primers 5'-ATGGAAGGTCCAGCGTTCT-3' and 5'-TTATTCACGCGATTCTACTTCT-3'. The resulting fragment was cloned into pLenti6 vector.

A validated Bcl2l11-specific shRNA sequence (TRC shRNA library, Sigma Aldrich) was integrated into the pLKO1 vector using sequence 5'-CGCGTCCGGGACGAGTTCAACGAACTTACCTCGAGGTAAGTTTCGTTGAACTCGTCTTTTTGGAAATTAC-3'. The sequence of the scrambled shRNA is 5'-CGCGTCCGGCAACAAGATGAAGAGCACCAACTCGAGTTGGTGCTCTTCATCTTGTGTTTTTGGAAA-3'.

For overexpression and shRNA knock-down, lentiviral particles were produced according to (Sadic et al., 2015) and used to transduce 3-4x10⁵ hematopoietic progenitors (lin⁻) pre-stimulated for 2 days with IL-7 (10ng/ml). Progenitors transduced with viruses carrying shRNA were kept in culture 24 h before seeding in MethoCult 3630 + 0,5 μ g/ml puromycin.

For overexpression assays, transduced cells were kept in culture for 3 days in RPMI supplemented with IL-7 (10ng/ml) before FACS analysis.

Acknowledgements

We thank Frank Malik for generously providing the 83A25 antibody and Marc Schmidt-Supprian for sharing the *Mbl-Cre* mice. Work in the G.S. lab was funded by the Deutsche Forschungsgemeinschaft (SFB684). L.K. was supported by the Deutsche Forschungsgemeinschaft. M.B. is supported by Boehringer Ingelheim and an ERC Advanced Grant (291740-LymphoControl) from the European Community's Seventh Framework Program. This work was also supported by a CNPq-Brazil fellowship to GP de Almeida (process number 204724/2013-9).

Author contributions

G.S., A.P., A.E., G.P.A., L.K., M.B. contributed to concepts and approaches; A.P., G.P.A., A.E., M.H., M.K., A.N., J.E. performed experiments; A.P., A.E., G.P.A., M.K., G.S. analyzed data; G.S. prepared the manuscript; A.P., A.E., G.P.A., L.K., M.B. edited the manuscript.

Conflict of interest

The authors declare no conflict of interest.

References

- Beguelin, W., Popovic, R., Teater, M., Jiang, Y., Bunting, K. L., Rosen, M., Shen, H., Yang, S. N., Wang, L., Ezponda, T., et al. (2013). EZH2 is required for germinal center formation and somatic EZH2 mutations promote lymphoid transformation. *Cancer cell* **23**, 677-692.
- Beissbarth, T. and Speed, T. P. (2004). GStat: find statistically overrepresented Gene Ontologies within a group of genes. *Bioinformatics* **20**, 1464-1465.
- Bilodeau, S., Kagey, M. H., Frampton, G. M., Rahl, P. B. and Young, R. A. (2009). SetDB1 contributes to repression of genes encoding developmental regulators and maintenance of ES cell state. *Genes & development* **23**, 2484-2489.
- Bourc'his, D. and Bestor, T. H. (2004). Meiotic catastrophe and retrotransposon reactivation in male germ cells lacking Dnmt3L. *Nature* **431**, 96-99.
- Brewer, J. W. and Hendershot, L. M. (2005). Building an antibody factory: a job for the unfolded protein response. *Nature immunology* **6**, 23-29.
- Brownlie, R. J., Lawlor, K. E., Niederer, H. A., Cutler, A. J., Xiang, Z., Clatworthy, M. R., Floto, R. A., Greaves, D. R., Lyons, P. A. and Smith, K. G. (2008). Distinct cell-specific control of autoimmunity and infection by FcγRIIb. *The Journal of experimental medicine* **205**, 883-895.
- Bulut-Karslioglu, A., De La Rosa-Velazquez, I. A., Ramirez, F., Barenboim, M., Onishi-Seebacher, M., Arand, J., Galan, C., Winter, G. E., Engist, B., Gerle, B., et al. (2014). Suv39h-dependent H3K9me3 marks intact retrotransposons and silences LINE elements in mouse embryonic stem cells. *Molecular cell* **55**, 277-290.
- Calton, M., Zeng, H., Urano, F., Till, J. H., Hubbard, S. R., Harding, H. P., Clark, S. G. and Ron, D. (2002). IRE1 couples endoplasmic reticulum load to secretory capacity by processing the XBP-1 mRNA. *Nature* **415**, 92-96.
- Collins, P. L., Kyle, K. E., Egawa, T., Shinkai, Y. and Oltz, E. M. (2015). The histone methyltransferase SETDB1 represses endogenous and exogenous retroviruses in B lymphocytes. *Proceedings of the National Academy of Sciences of the United States of America* **112**, 8367-8372.
- Dodge, J. E., Kang, Y. K., Beppu, H., Lei, H. and Li, E. (2004). Histone H3-K9 methyltransferase ESET is essential for early development. *Molecular and cellular biology* **24**, 2478-2486.
- Egle, A., Harris, A. W., Bath, M. L., O'Reilly, L. and Cory, S. (2004). VavP-Bcl2 transgenic mice develop follicular lymphoma preceded by germinal center hyperplasia. *Blood* **103**, 2276-2283.
- Evans, L. H., Morrison, R. P., Malik, F. G., Portis, J. and Britt, W. J. (1990). A neutralizable epitope common to the envelope glycoproteins of ecotropic, polytropic, xenotropic, and amphotropic murine leukemia viruses. *Journal of virology* **64**, 6176-6183.
- Finstad, S. L., Rosenberg, N. and Levy, L. S. (2007). Diminished potential for B-lymphoid differentiation after murine leukemia virus infection in vivo and in EML hematopoietic progenitor cells. *Journal of virology* **81**, 7274-7279.
- Gass, J. N., Gunn, K. E., Sriburi, R. and Brewer, J. W. (2004). Stressed-out B cells? Plasma-cell differentiation and the unfolded protein response. *Trends in immunology* **25**, 17-24.
- Groenendyk, J., Peng, Z., Dudek, E., Fan, X., Mizianty, M. J., Dufey, E., Urrea, H.,

- Sepulveda, D., Rojas-Rivera, D., Lim, Y., et al.** (2014). Interplay between the oxidoreductase PDIA6 and microRNA-322 controls the response to disrupted endoplasmic reticulum calcium homeostasis. *Science signaling* **7**, ra54.
- Hardy, R. R., Carmack, C. E., Shinton, S. A., Kemp, J. D. and Hayakawa, K.** (1991). Resolution and characterization of pro-B and pre-pro-B cell stages in normal mouse bone marrow. *The Journal of experimental medicine* **173**, 1213-1225.
- Heng, T. S., Painter, M. W. and Immunological Genome Project, C.** (2008). The Immunological Genome Project: networks of gene expression in immune cells. *Nature immunology* **9**, 1091-1094.
- Hobeika, E., Thiemann, S., Storch, B., Jumaa, H., Nielsen, P. J., Pelanda, R. and Reth, M.** (2006). Testing gene function early in the B cell lineage in mb1-cre mice. *Proceedings of the National Academy of Sciences of the United States of America* **103**, 13789-13794.
- Holmes, R. and Zuniga-Pflucker, J. C.** (2009). The OP9-DL1 system: generation of T-lymphocytes from embryonic or hematopoietic stem cells in vitro. *Cold Spring Harbor protocols* **2009**, pdb.prot5156.
- Jojic, V., Shay, T., Sylvia, K., Zuk, O., Sun, X., Kang, J., Regev, A., Koller, D., Immunological Genome Project, C., Best, A. J., et al.** (2013). Identification of transcriptional regulators in the mouse immune system. *Nature immunology* **14**, 633-643.
- Karimi, M. M., Goyal, P., Maksakova, I. A., Bilenky, M., Leung, D., Tang, J. X., Shinkai, Y., Mager, D. L., Jones, S., Hirst, M., et al.** (2011). DNA methylation and SETDB1/H3K9me3 regulate predominantly distinct sets of genes, retroelements, and chimeric transcripts in mESCs. *Cell stem cell* **8**, 676-687.
- Lawson, K. A., Teteak, C. J., Gao, J., Li, N., Hacquebord, J., Ghatan, A., Zielinska-Kwiatkowska, A., Song, G., Chansky, H. A. and Yang, L.** (2013). ESET histone methyltransferase regulates osteoblastic differentiation of mesenchymal stem cells during postnatal bone development. *FEBS letters* **587**, 3961-3967.
- Lee, A. S.** (2005). The ER chaperone and signaling regulator GRP78/BiP as a monitor of endoplasmic reticulum stress. *Methods* **35**, 373-381.
- Lee, E., Iskow, R., Yang, L., Gokcumen, O., Haseley, P., Luquette, L. J., 3rd, Lohr, J. G., Harris, C. C., Ding, L., Wilson, R. K., et al.** (2012). Landscape of somatic retrotransposition in human cancers. *Science* **337**, 967-971.
- Martin, F. J., Xu, Y., Lohmann, F., Ciccone, D. N., Nicholson, T. B., Loureiro, J. J., Chen, T. and Huang, Q.** (2015). KMT1E-mediated chromatin modifications at the EcgammaRIIb promoter regulate thymocyte development. *Genes and immunity*.
- Matsui, T., Leung, D., Miyashita, H., Maksakova, I. A., Miyachi, H., Kimura, H., Tachibana, M., Lorincz, M. C. and Shinkai, Y.** (2010). Proviral silencing in embryonic stem cells requires the histone methyltransferase ESET. *Nature* **464**, 927-931.
- Puthalakath, H., O'Reilly, L. A., Gunn, P., Lee, L., Kelly, P. N., Huntington, N. D., Hughes, P. D., Michalak, E. M., McKimm-Breschkin, J., Motoyama, N., et al.** (2007). ER stress triggers apoptosis by activating BH3-only protein Bim. *Cell* **129**, 1337-1349.
- Regha, K., Sloane, M. A., Huang, R., Pauler, F. M., Warczok, K. E., Melikant, B., Radolf, M., Martens, J. H., Schotta, G., Jenuwein, T., et al.** (2007). Active and repressive chromatin are interspersed without spreading in an imprinted gene cluster in the mammalian genome. *Molecular cell* **27**, 353-366.
- Revilla, I. D. R., Bilic, I., Vilagos, B., Tagoh, H., Ebert, A., Tamir, I. M., Smeenk, L., Trupke, J., Sommer, A., Jaritz, M., et al.** (2012). The B-cell identity factor Pax5 regulates distinct transcriptional programmes in early and late B lymphopoiesis. *The*

EMBO journal **31**, 3130-3146.

- Roulois, D., Loo Yau, H., Singhania, R., Wang, Y., Danesh, A., Shen, S. Y., Han, H., Liang, G., Jones, P. A., Pugh, T. J., et al.** (2015). DNA-Demethylating Agents Target Colorectal Cancer Cells by Inducing Viral Mimicry by Endogenous Transcripts. *Cell* **162**, 961-973.
- Sadic, D., Schmidt, K., Groh, S., Kondofersky, I., Ellwart, J., Fuchs, C., Theis, F. J. and Schotta, G.** (2015). Atrx promotes heterochromatin formation at retrotransposons. *EMBO Rep* **16**, 836-850.
- Santoni de Sio, F. R., Massacand, J., Barde, I., Offner, S., Corsinotti, A., Kapopoulou, A., Bojkowska, K., Dagklis, A., Fernandez, M., Ghia, P., et al.** (2012). KAP1 regulates gene networks controlling mouse B-lymphoid cell differentiation and function. *Blood* **119**, 4675-4685.
- Schwickert, T. A., Tagoh, H., Gultekin, S., Dakic, A., Axelsson, E., Minnich, M., Ebert, A., Werner, B., Roth, M., Cimmino, L., et al.** (2014). Stage-specific control of early B cell development by the transcription factor Ikaros. *Nature immunology* **15**, 283-293.
- Su, I. H., Basavaraj, A., Krutchinsky, A. N., Hobert, O., Ullrich, A., Chait, B. T. and Tarakhovsky, A.** (2003). Ezh2 controls B cell development through histone H3 methylation and IgH rearrangement. *Nature immunology* **4**, 124-131.
- Tan, S. L., Nishi, M., Ohtsuka, T., Matsui, T., Takemoto, K., Kamio-Miura, A., Aburatani, H., Shinkai, Y. and Kageyama, R.** (2012). Essential roles of the histone methyltransferase ESET in the epigenetic control of neural progenitor cells during development. *Development* **139**, 3806-3816.
- Xie, D., Chen, C. C., Ptaszek, L. M., Xiao, S., Cao, X., Fang, F., Ng, H. H., Lewin, H. A., Cowan, C. and Zhong, S.** (2010). Rewirable gene regulatory networks in the preimplantation embryonic development of three mammalian species. *Genome research* **20**, 804-815.
- Xie, M., Hong, C., Zhang, B., Lowdon, R. F., Xing, X., Li, D., Zhou, X., Lee, H. J., Maire, C. L., Ligon, K. L., et al.** (2013). DNA hypomethylation within specific transposable element families associates with tissue-specific enhancer landscape. *Nature genetics* **45**, 836-841.
- Yang, L., Lawson, K. A., Teteak, C. J., Zou, J., Hacquebord, J., Patterson, D., Ghatan, A. C., Mei, Q., Zielinska-Kwiatkowska, A., Bain, S. D., et al.** (2013). ESET histone methyltransferase is essential to hypertrophic differentiation of growth plate chondrocytes and formation of epiphyseal plates. *Developmental biology* **380**, 99-110.
- Young, G. R., Eksmond, U., Salcedo, R., Alexopoulou, L., Stoye, J. P. and Kassiotis, G.** (2012). Resurrection of endogenous retroviruses in antibody-deficient mice. *Nature* **491**, 774-778.
- Yuan, P., Han, J., Guo, G., Orlov, Y. L., Huss, M., Loh, Y. H., Yaw, L. P., Robson, P., Lim, B. and Ng, H. H.** (2009). Eset partners with Oct4 to restrict extraembryonic trophoblast lineage potential in embryonic stem cells. *Genes & development* **23**, 2507-2520.
- Zhang, K., Wong, H. N., Song, B., Miller, C. N., Scheuner, D. and Kaufman, R. J.** (2005). The unfolded protein response sensor IRE1alpha is required at 2 distinct steps in B cell lymphopoiesis. *J Clin Invest* **115**, 268-281.
- Zhao, X. and Yoshimura, F. K.** (2008). Expression of murine leukemia virus envelope protein is sufficient for the induction of apoptosis. *Journal of virology* **82**, 2586-2589.

Figures

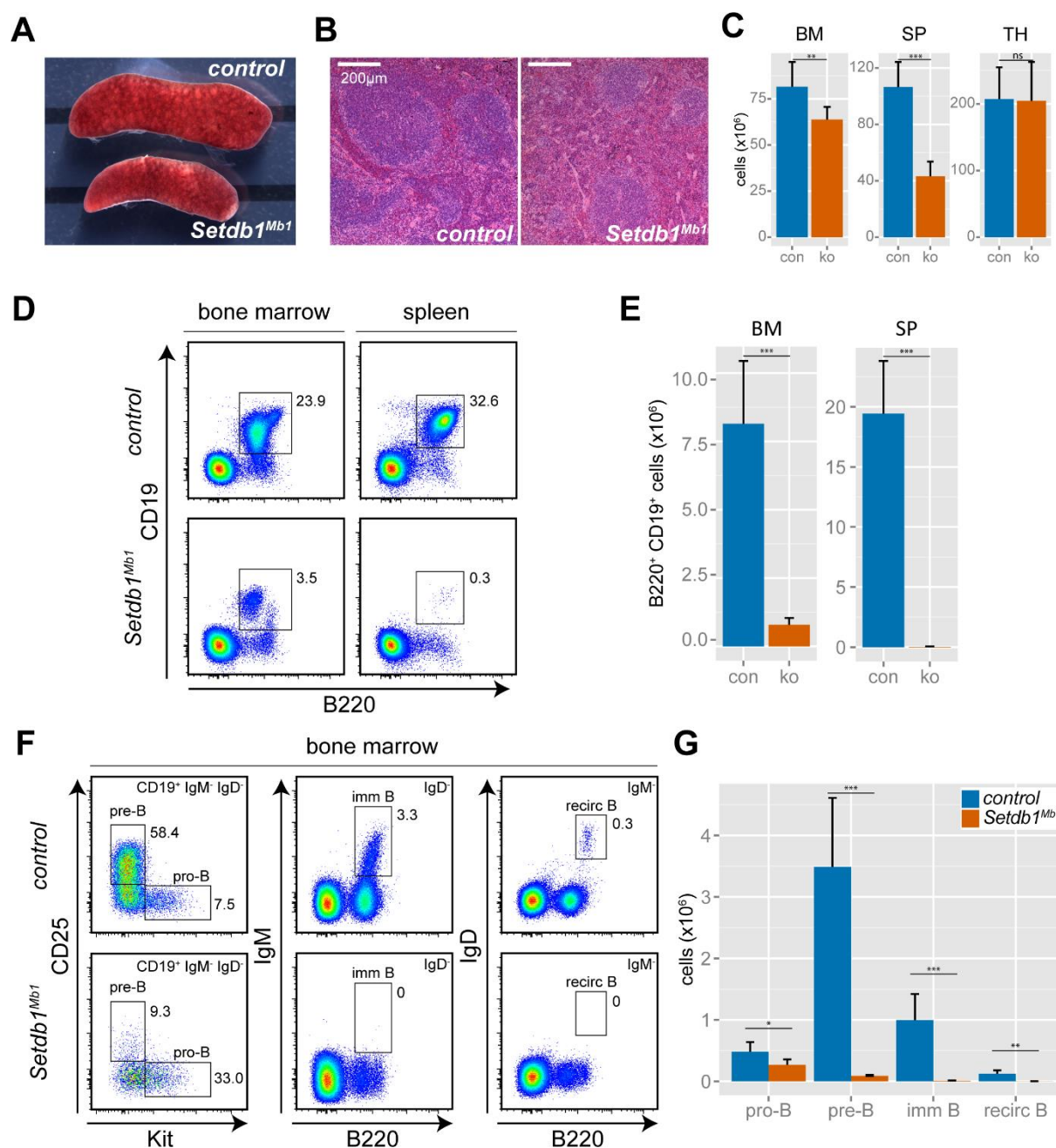


Figure 1. Loss of *Setdb1* in early B cells leads to impaired B cell development.

(A) Spleen of *control* and *Setdb1^{Mb1}* mice.

(B) Paraffin sections of *control* and *Setdb1^{Mb1}* spleen stained with hematoxylin/eosin. Areas with dark blue staining are follicles with accumulation of lymphocytes.

(C) Total cell numbers of bone marrow (BM), spleen (SP) and thymus (TH) in *control* (con)

and *Setdb1*^{Mbl} (ko) mice (n=6). **P < 0.01 and ***P < 0.001 (unpaired two-tailed Student's t-test).

(D) Representative FACS plots showing the B cell population (B220⁺ CD19⁺) in spleen and bone marrow of *control* (con) and *Setdb1*^{Mbl} (ko) mice.

(E) Bargraph showing the average total numbers of B220⁺ CD19⁺ B cells in *control* (con) and *Setdb1*^{Mbl} (ko) mice (n=6). **P < 0.01 and ***P < 0.001 (unpaired two-tailed Student's t-test).

(F) Representative FACS plot showing different stages of B cell development in the bone marrow of *control* and *Setdb1*^{Mbl} mice.

(G) Bargraph showing average total cell numbers of B cell developmental stages in bone marrow from *control* (con) and *Setdb1*^{Mbl} (ko) mice (n=6). **P < 0.01 and ***P < 0.001 (unpaired two-tailed Student's t-test).

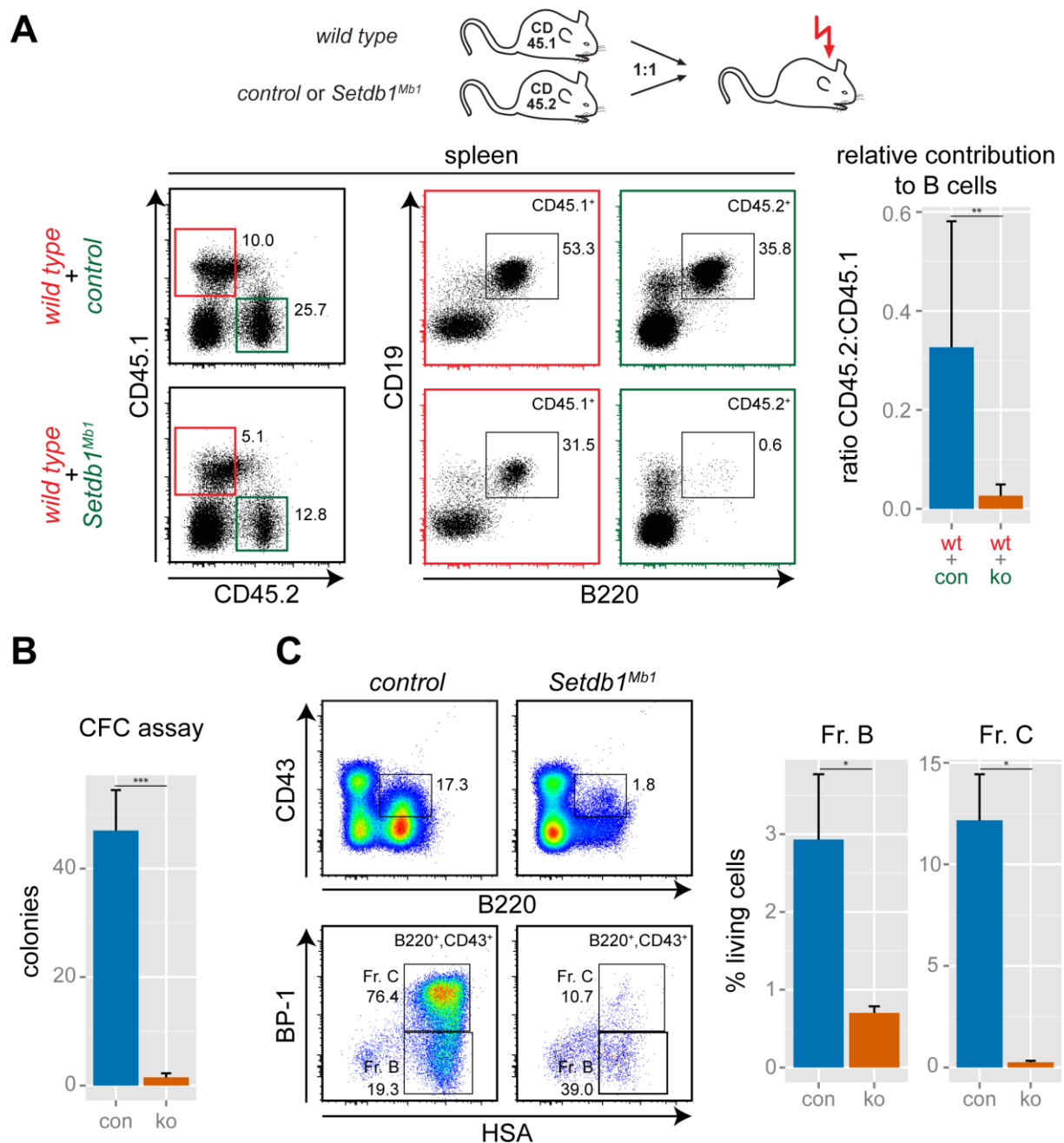


Figure 2. *Setdb1* has cell-intrinsic functions for B cell development.

(A) Schematic representation of the bone marrow transplantation strategy (top). Representative FACS plots showing the relative contribution to the B cell lineage of wild type vs. *control* or *Setdb1*^{Mb1} donor bone marrow. Bargraph shows the quantification (n=3) of splenic B cells (B220⁺ CD19⁺) in recipient mice as ratio between *control* (con) or *Setdb1*^{Mb1} (ko) to wild type (wt). **P < 0.01 (unpaired two-tailed Student's t-test).

(B) Colony formation assay in Methocult 3630 to support B cell colony formation. Bargraph depicts the average colony number of three independent experiments with *control* (con) and

Setdb1^{Mb1} (ko) bone marrow cells (n=3). ***P < 0.001 (unpaired two-tailed Student's t-test).

(C) Representative FACS analysis of differentiated B cells (CD43⁺ B220⁺) after 8 days of OP9 co-culture in the presence of Il-7. Bargraph shows quantification of 3 independent experiments for Fr. B (B220⁺ CD43⁺ HSA⁺ BP-1⁻) and Fr. C (B220⁺ CD43⁺ HSA⁺ BP-1⁺) B cells. *P < 0.05 (unpaired two-tailed Student's t-test).

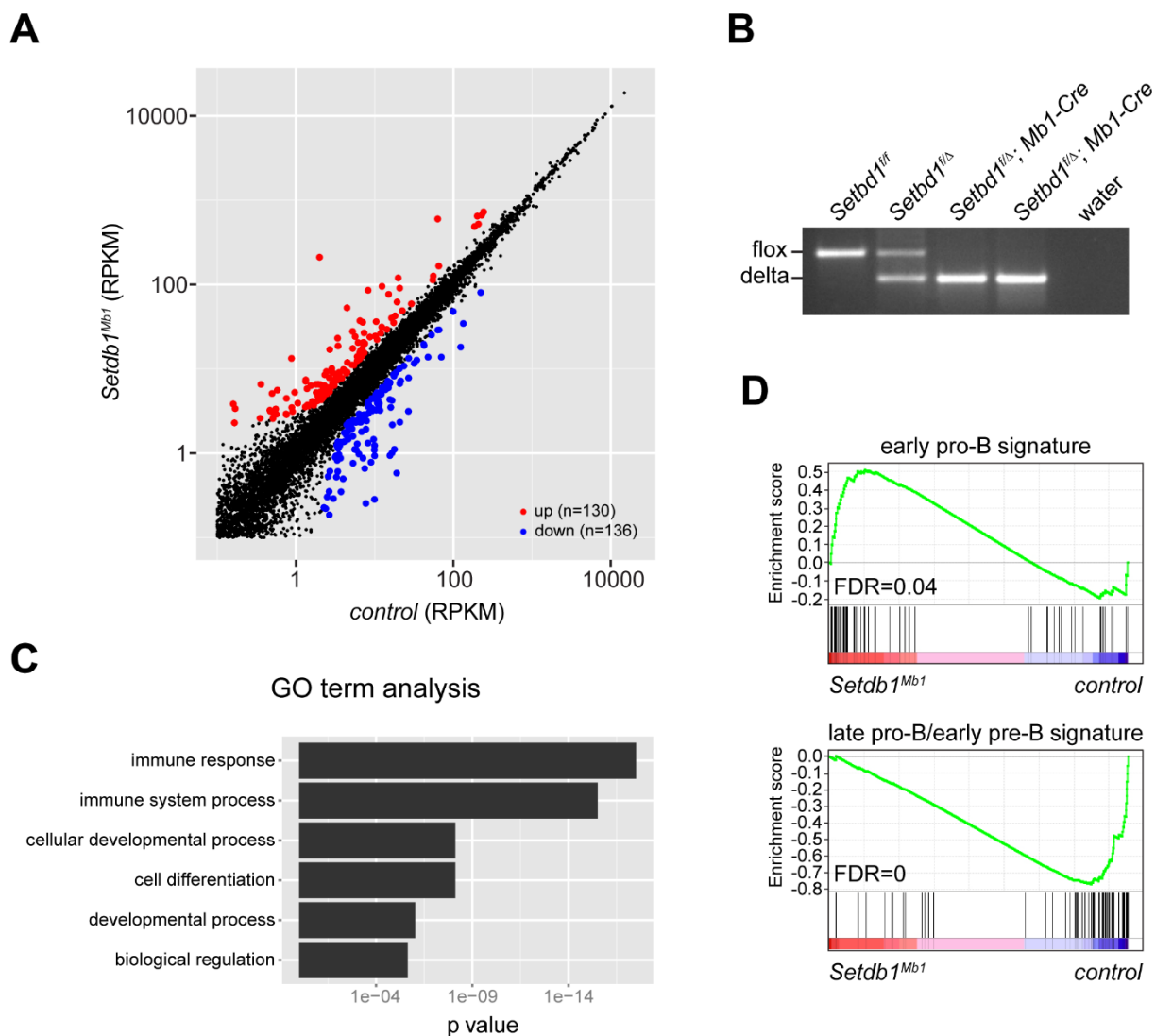


Figure 3. Transcriptome analysis of *Setdb1*^{Mb1} pro-B cells revealed impaired pro-B to pre-B cell transition.

(A) RNA-Seq analysis performed on sorted *control* and *Setdb1*^{Mb1} pro-B cells (CD19⁺ IgD⁻ IgM⁻ Kit⁺ CD25⁻). Correlation plot shows expression levels of all genes in *control* and *Setdb1*-deficient pro-B cells as normalized RNA-seq read coverage in reads per kilobase per million reads (RPKM). Red dots – upregulated genes, blue dots – down-regulated genes, black dots – genes less than 2-fold regulated.

(B) Deletion efficiency of the floxed *Setdb1* allele in pro-B cells was determined by PCR on genomic DNA. In *Setdb1*^{Mb1} (*Setdb1*^{flox/delta}; *mb1-Cre*) pro-B cells, absence of the flox band indicates complete deletion of the floxed exon 4.

(C) GO term enrichment analysis of the dysregulated genes in *Setdb1*^{Mb1} pro-B cells was performed with GOSTat (Beissbarth and Speed, 2004). P-values of the most highly enriched terms are plotted.

(D) Gene set enrichment analysis of RNA-seq data from *control* and *Setdb1^{Mbl}* pro-B cells with gene lists representing Hardy Fr. A (B220⁺ CD43⁺ HSA^{low} BP-1⁻) and Fr. B/C (B220⁺ CD43⁺ HSA^{high}). *Setdb1^{Mbl}* pro-B cells displayed a clear enrichment for the Fr. A signature, while Fr. B/C signatures were depleted. FDR – false discovery rate.

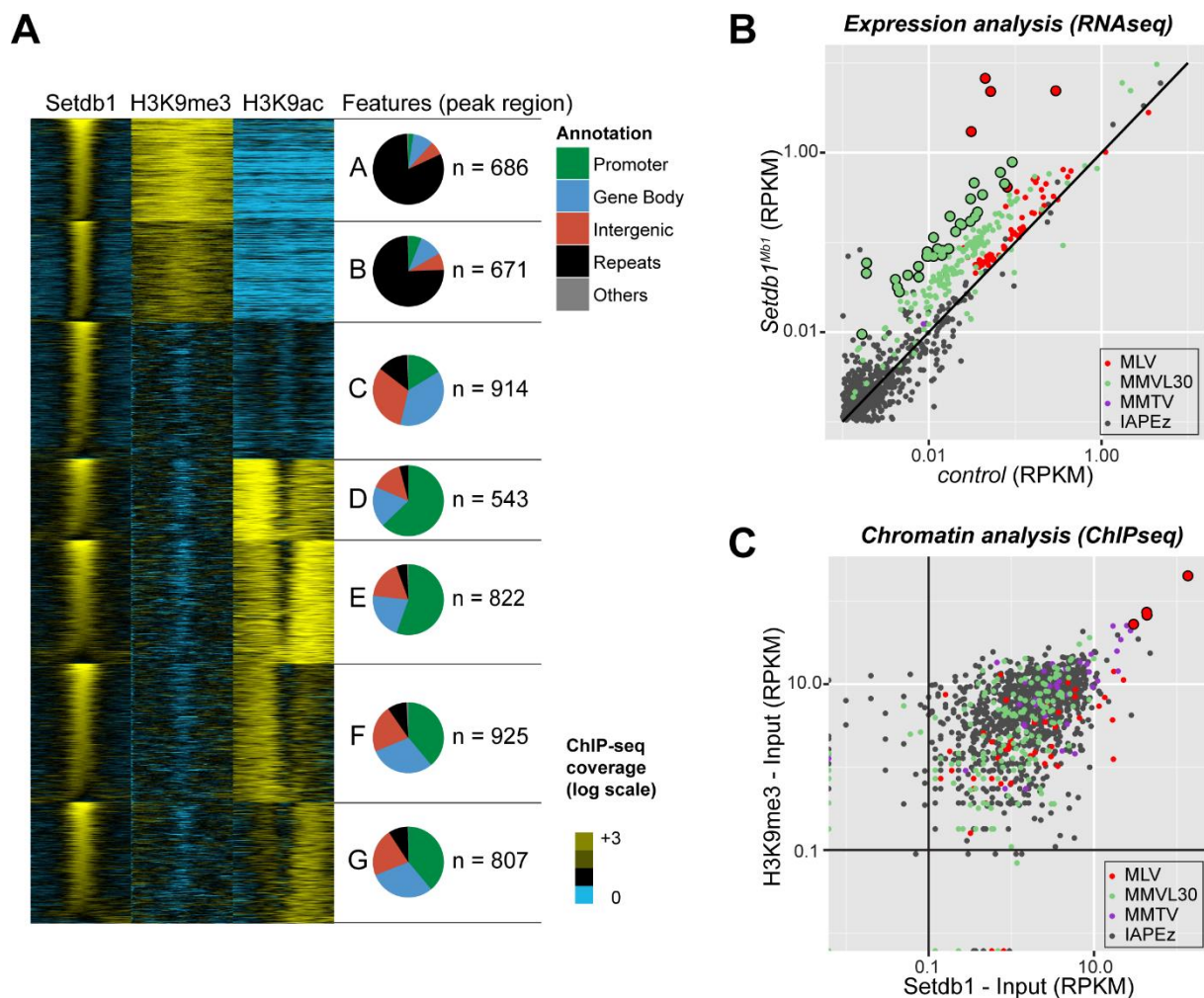


Figure 4. Setdb1 directly silences repetitive elements in pro-B cells.

(A) ChIP-Seq analysis for Setdb1, H3K9me3 and H3K9ac in short-term cultured *Rag2*^{-/-} pro-B cells. Heatmap shows log-transformed read coverage for Setdb1 and H3K9 modifications 1500 bp across all Setdb1 binding sites. Peak clusters were generated based on H3K9me3/H3K9ac occupancy using Cluster3 software. Pie charts depict the frequency of genomic features at Setdb1 peaks in each cluster.

(B) Double log scatter plot of normalized RNA-seq read coverage (RPKM) over distinct retrotransposon sequences in *control* and *Setdb1*^{Mb1} pro-B cells. Large dots depict retrotransposons with > 5 fold expression changes. Strongest upregulation in *Setdb1*^{Mb1} pro-B cells was found for four MLV elements (large red dots).

(C) Double log scatter plot of normalized ChIP-seq read coverage minus Input (RPKM) for Setdb1 and H3K9me3 over distinct retrotransposons. The four MLV retrotransposons with the highest expression changes (B) are shown as large red dots.

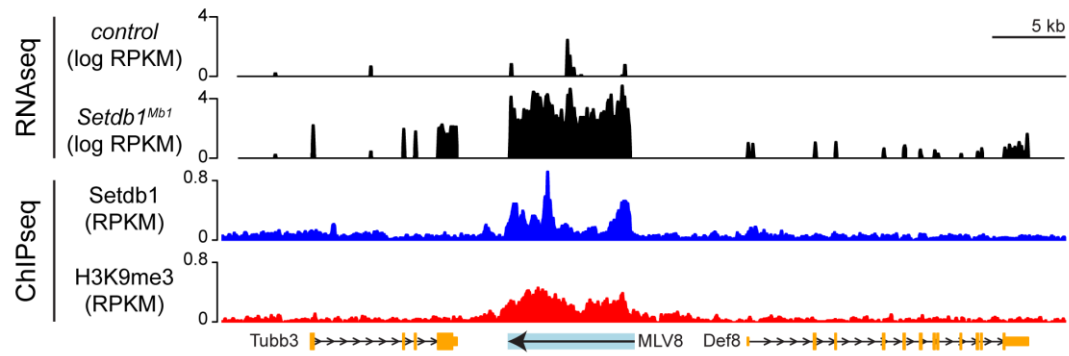
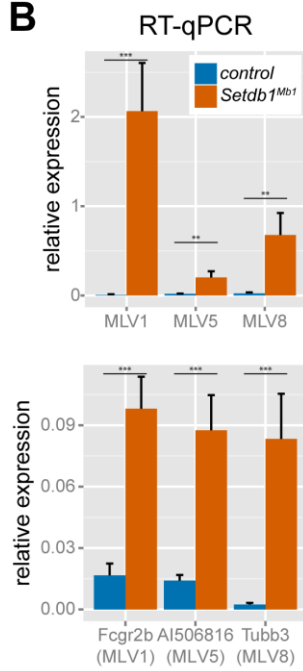
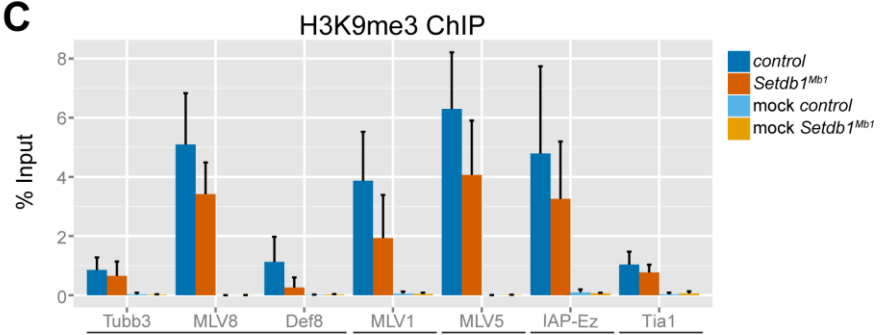
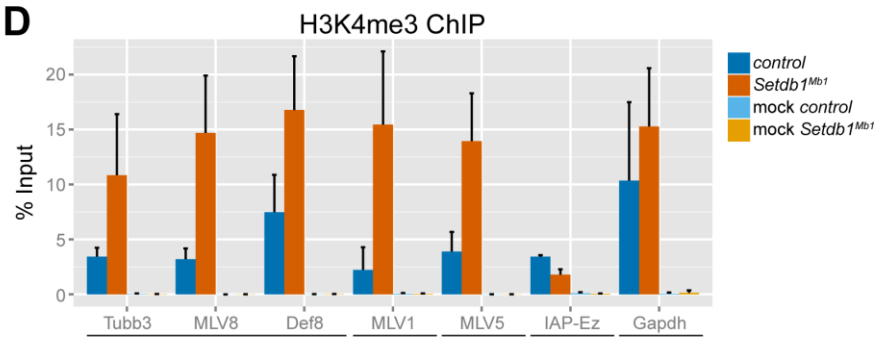
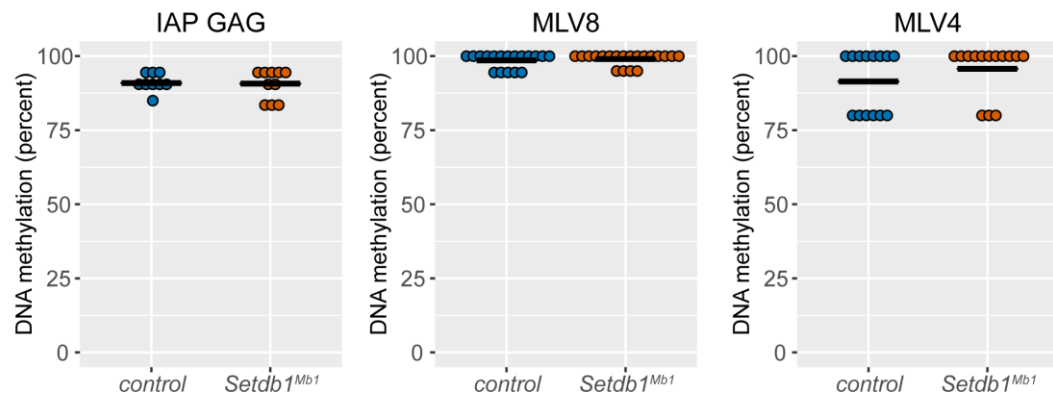
A**B****C****D****E**

Figure 5. Setdb1 directly regulates MLV silencing by preventing establishment of active H3K4me3.

(A) Coverage plot of normalized RNA-seq (*control* vs. *Setdb1^{Mb1}* pro-B cells) and ChIP-seq (short-term cultured *Rag2^{-/-}* pro-B cells) coverage across the genomic region of MLV8.

(B) Quantitative RT-PCR on the three most derepressed MLVs (left) and genes in their respective vicinity (right). Gene expression was calculated as relative expression to housekeeping genes from 6 biological replicates. **P < 0.01 and ***P < 0.001 (unpaired two-tailed Student's t-test).

(C) ChIP-qPCR (n=3) for H3K9me3 in *control* and *Setdb1^{Mb1}* pro-B cells on MLV retrotransposons and promoter regions of genes in their respective vicinity. IAP-ez – consensus primer set for IAP-ez elements (positive control), Tia1 – primer set for the promoter of the Tia1 gene (negative control).

(D) ChIP-qPCR (n=3) for H3K4me3 in *control* and *Setdb1^{Mb1}* pro-B cells on MLV retrotransposons and promoter regions of genes in their respective vicinity. IAP-ez – consensus primer set for IAP-ez elements (negative control), Gapdh – primer set for the promoter of the Gapdh gene (positive control).

(E) DNA methylation of IAP GAG (no transcriptional change), MLV8 (derepressed) and MLV4 (no transcriptional change) was analyzed by bisulfite sequencing in control and *Setdb1^{Mb1}* pro-B cells. Plots show quantification of the DNA methylation analysis.

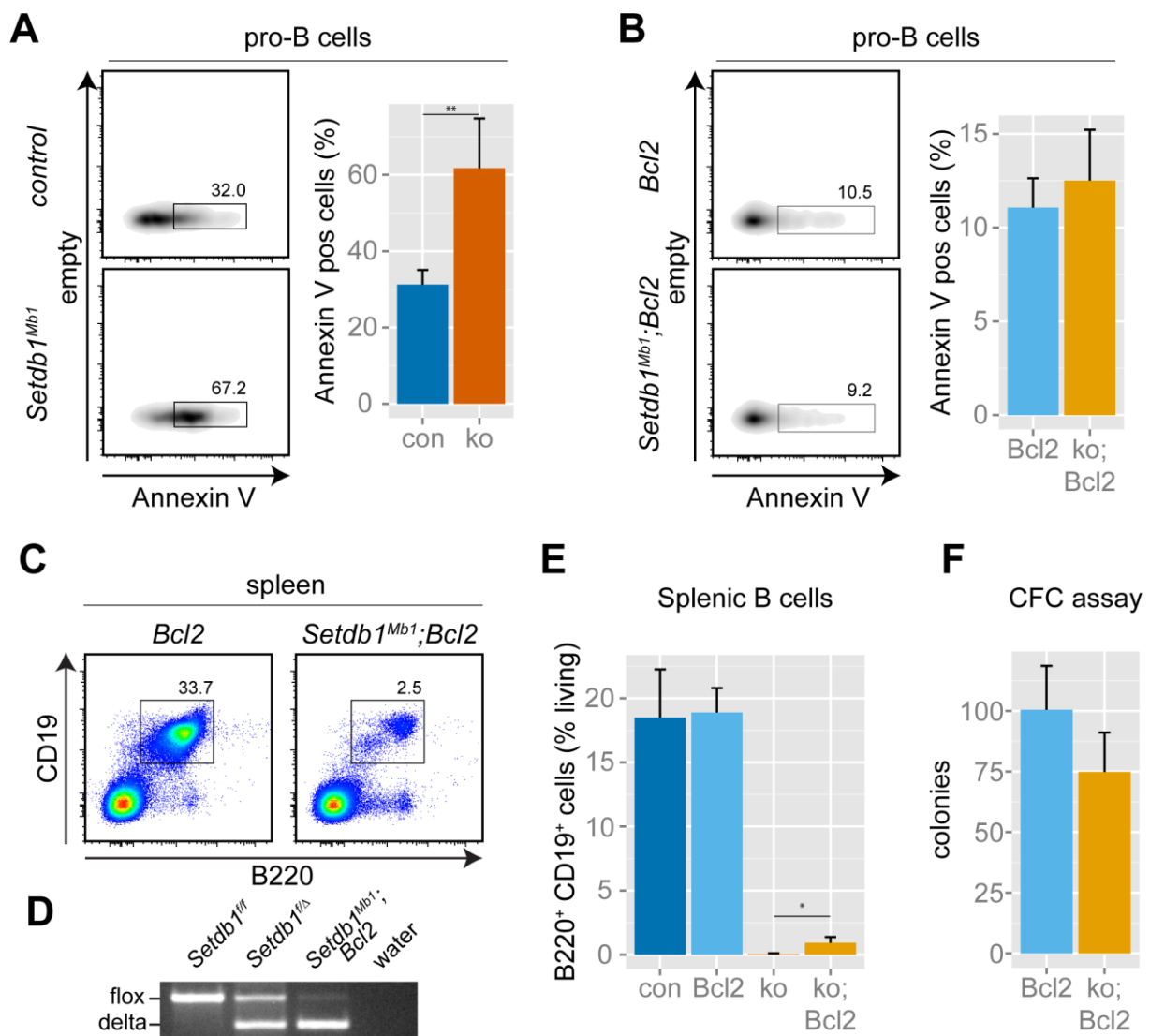


Figure 6. *Setdb1*^{Mb1} pro-B cells die from apoptosis.

(A) Apoptosis in *control* (con) and *Setdb1*^{Mb1} (ko) pro-B cells (CD19⁺ IgM⁻ IgD⁻ CD25⁻ Kit⁺) was measured by Annexin V staining. Average percentage of Annexin V positive pro-B cells from 6 biological replicates are displayed in the bargraph. **P < 0.01 (unpaired two-tailed Student's t-test).

(B) Apoptosis in *Bcl2* and *Setdb1*^{Mb1}; *Bcl2* pro-B cells (CD19⁺ IgM⁻ IgD⁻ CD25⁻ Kit⁺) was measured by Annexin V staining. Average percentage of Annexin V positive pro-B cells from 6 biological replicates are displayed in the bargraph.

(C) Representative FACS analyses of splenic B cells (CD19⁺ B220⁺) in *Bcl2* and *Setdb1*^{Mb1}; *Bcl2* mice.

(D) *Setdb1* deletion rate monitored in sorted splenic B cells (IgM⁺ IgD⁺) by PCR.

(E) Bargraph depicts average percentages of splenic B cells from *control*, *Bcl2*, *Setdb1*^{Mb1} and

Setdb1^{Mb1}; Bcl2 mice (n=6). *P < 0.05 (unpaired two-tailed Student's t-test).

(F) Colony formation assay in Methocult 3630 for pre-B cell colony formation. Bargraph depicts the average colony number of three independent experiments with *control* (Bcl2) and *Setdb1^{Mb1}; Bcl2* (ko; Bcl2) bone marrow cells.

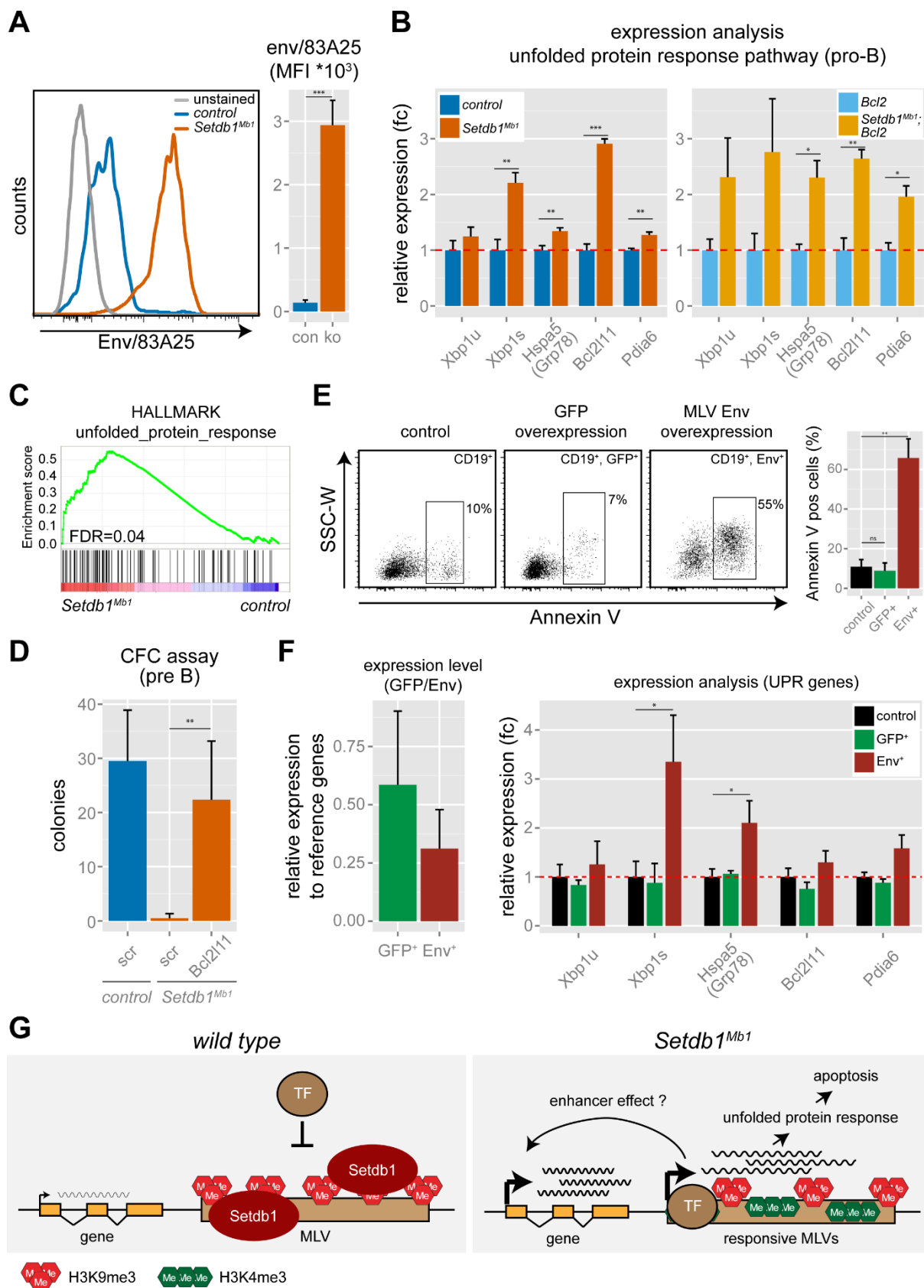


Figure 7. Strong expression of MLV proteins leads to UPR-mediated apoptosis.

(A) MLV envelope protein expression detected by FACS on *control* (con) and *Setdb1^{Mb1}* (ko) pro-B cells (CD19⁺ IgM⁻ IgD⁻ Kit⁺). Bargraph depicts the average env expression calculated

as mean fluorescence intensity (MFI) from 6 mice per genotype. *** $P < 0.001$ (unpaired two-tailed Student's t-test).

(B) RT-qPCR expression analyses of main UPR genes. Bargraph shows fold change gene expression of *Setdb1*^{Mbl} over *control* (left panel) and *Setdb1*^{Mbl}; *Bcl2* over *Bcl2* (right panel) pro-B cells (CD19⁺ IgM⁻ IgD⁻ CD25⁻ Kit⁺). * $P < 0.05$ (unpaired two-tailed Student's t-test). Xbp1u – Xbp1 normal splice form; Xbp1s – Xbp1 UPR-related splice isoform; Hspa5, Bcl2l11, Pdia6 – major mediators of the UPR response.

(C) Gene set enrichment analysis of RNA-seq data from *control* and *Setdb1*^{Mbl} pro-B cells using the hallmarks gene sets (MySigDB) revealed significant enrichment for the unfolded protein response gene set. FDR – false discovery rate.

(D) Colony formation assay in Methocult 3630 for pre-B cell colony formation. Bargraph depicts the average colony number of three independent experiments with *control* and *Setdb1*^{Mbl} bone marrow cells infected with scrambled or Bcl2l11-specific shRNAs. ** $P < 0.005$ (unpaired two-tailed Student's t-test).

(E) Overexpression of MLV Env protein induces apoptosis. Lineage negative bone marrow cells (non-infected, GFP infected and MLV Env infected) were differentiated into B cells and apoptosis was measured by Annexin V staining. ** $P < 0.005$, n.s. – not significant (unpaired two-tailed Student's t-test).

(F) Overexpression of MLV Env protein induces UPR genes. left panel: RT-qPCR analysis of samples from (E) for expression levels of GFP and Env based on a common part of their transcripts. right panel: RT-qPCR expression analyses of main UPR genes in samples from (E). Bargraph shows fold change gene expression of GFP⁺ or Env⁺ B cells over non transfected control cells. * $P < 0.05$ (unpaired two-tailed Student's t-test).

(G) Model. In wild type pro-B cells, Setdb1 is recruited to retrotransposons and establishes H3K9me3. This presumably prevents the access for transcription factors which have binding sites within the retrotransposon sequence. In *Setdb1*^{Mbl} pro-B cells, loss of Setdb1 leads to accumulation of H3K4me3 and strong transcription of retrotransposon sequences. MLV transcripts are translated and lead to the massive production of MLV envelope protein. This triggers activation of the unfolded protein response and apoptosis of pro-B cells. Derepressed retrotransposons also act as enhancers and lead to strong transactivation of genes in their vicinity.

Supplementary Materials and Methods

Setdb1 genotyping

To detect floxed and wild type *Setdb1* alleles primers spanning the floxed region were used (5'-TGCCCCCACCACCTTTATAC-3' (F), 5'-AAACACTCCCCCAGACAG-3' (R)). PCR amplification generated 2 fragments of 600 bp and 500 bp which corresponded to *Setdb1* floxed and *Setdb1* wild type alleles, respectively. To identify presence of the *Setdb1* delta allele the following primers were used: 5'-TGCCCCCACCACCTTTATAC-3' (F) and 5'-AGTAAATCTTTGAGCCAGAGCAAGC-3' (R), resulting in a 350 bp PCR amplicon. The *Mbl-Cre* allele was detected using the following primer pair: 5'-CCCTGTGGATGCCACCTC-3' (F) and 5'-GTCCTGGCATCTGTCAGAG-3' (R). *Vav-bcl2* was detected using primers 5'-ACGGTGGTGGAGGAGCTCTTC-3' (F) and 5'-AAAACCTCCCACACCTCCCCCTGAA-3' (R).

Chromatin immunoprecipitation

For ChIP-qPCR 1×10^6 sorted cells were fixed using 1% formaldehyde. Fixation was stopped by adding glycine (final concentration 0.125M). Fixed cells were washed twice by rotation using PBS 10% FCS. After the last wash, pellets were flash frozen.

Cells were lysed by adding buffer B (50 mM Tris-HCl pH 8.0, 10 mM EDTA, 1% SDS). Lysates were then transferred to AFA Fiber microtubes with Snap-Cap and sonicated using Covaris E220 for 20 minutes at 4°C.

For the immunoprecipitation step α -H3K9me3 (Activ Motif, #39161.39162, lot #13509002) and α -H3K4me3 (Diagenode, #pAB-003-050, lot #A49-001 and #CS-003-100, lot #A5051-001P) antibodies were bound to magnetic Dynabeads (Applied technology). Next, sheared chromatin was diluted in buffer A (10 mM Tris HCl pH 7.5, 1 mM EDTA, 0.5 mM EGTA, 1% Triton 100 X, 0.1% SDS, 0.1% Na-deoxycholate, 140 mM NaCl) and incubated with the appropriate antibody-conjugated beads for 4 hours at 4°C on a rotator. Immunoprecipitated material was first washed 3 times with buffer A and then once with buffer C (10 mM Tris-HCl pH 8.0, 10 mM EDTA). Buffer A, B and C were all provided with protease inhibitor cocktail (Roche). Chromatin was then resuspended in elution buffer (50 mM Tris-HCl pH 8.0, 10 mM EDTA, 1% SDS) and incubated at 65°C on a mixer for 20 minutes. Eluted chromatin was next incubated overnight at 65°C for reverse cross-linking. Chromatin samples were treated with

RNase A and proteinase K and cleaned by phenol/chloroform purification. This material was subsequently used for qRT-PCR quantification with SYBR Green.

RNA-seq analysis

RNA-seq reads were mapped to the mouse genome (mm10) using tophat2 (Kim et al., 2013). Expression of genes in RPKM was calculated with cuffdiff and cummerbund (Trapnell et al., 2013). Dot plots were generated with ggplot2 (REF). GO term analysis of differentially expressed genes was performed with GStat (Beissbarth and Speed, 2004). For gene set enrichment analysis (Mootha et al., 2003; Subramanian et al., 2005) of differentially expressed genes custom gene lists for fraction A and fraction B/C specific genes were generated based on expression data from the ImmGen consortium.

For expression analysis of individual repeat elements, RNA-seq reads were mapped to the genome using bowtie (Langmead et al., 2009). Coverage across repeat families and individual repeats was analyzed using analyzeRepeats (Heinz et al., 2010). To identify individual MLV repeats we extracted all MLV elements from the rmsk database (UCSC) and quantified normalized RNA-seq read coverage using analyzeRepeats.pl. The four top-regulated MLV repeats display a >10 fold change in expression (control vs. *Setdb1*^{Mb1}; see Supplementary Table S3).

DNA methylation analysis

Genomic DNA from control and *Setdb1*^{Mb1} pro-B cells was subjected to bisulfite conversion using the EpiTect Bisulfite Kit™ (Qiagen) according to the manufacturer's protocol. Target regions were amplified by PCR, subcloned into pBluescript-SK2+ (Stratagene) and analyzed by Sanger sequencing. Methylation analysis of sequencing data was performed using BiQ Analyzer (Bock et al., 2005).

ChIP-seq analysis

Paired end ChIP-seq reads were mapped to the mouse genome (mm10) using bowtie (Langmead et al., 2009). Reads mapping to multiple locations were discarded. *Setdb1* peaks were identified using MACS (Zhang et al., 2008) and PeakRanger (Feng et al., 2011). Coverage across *Setdb1* peaks was calculated using homer (Heinz et al., 2010). Cluster

analysis was performed using cluster3 (de Hoon et al., 2004) and visualized with Java TreeView (Saldanha, 2004).

V-DJ recombination

Pro-B cells (Kit⁺ CD19⁺ IgM⁻ IgD⁻) were isolated from bone marrow of *control* (n=3), *Setdb1^{Mb1}* (n=3), *Bcl2* (n=1) and *Setdb1^{Mb1}; Bcl2* (n=1) mice using FACS Aria cell sorter. Genomic DNA was prepared from these cells using standard procedures. The analysis of V-DJ recombination was done by a PCR based assay as described (Fuxa et al., 2004).

Definition of hematopoietic cell types

For better definition of the hematopoietic populations cell doublets were excluded. Cell population analysis of transplanted mice was performed using the same marker scheme shown above with the implementation of CD45.1 and CD45.2 markers to discriminate donor bone marrows. Lineage negative cells (lin⁻) were detected using the following PE labeled antibody cocktail: CD45R/B220, CD5, CD19, CD11c, CD8a, CD4, Ly-6G (Gr-1), CD3e, CD19, CD11b(Mac-1).

For cell sorting, we used the marker combination to detect pro-B cells. Alternatively we sorted CD43⁺ CD19⁺ cell population (pro-B and pre-B cells), to perform ChIP-qPCR. IgD⁺ IgM⁺ cells were also sorted from *Setdb1^{Mb1}; Bcl2* spleen to check the deletion rate in the peripheral mature B cells.

Envelope protein and Fcγr2b staining

To detect the MLV envelope protein on pro-B cells, 4x10⁶ bone marrow cells were resuspended in a volume of 50 µl and incubated 30 minutes at RT with rat α-env (83A25) diluted 1:5. Subsequently cells were incubated for 1 hour at RT with an anti-rat secondary antibody conjugated Alexa-647. Bone marrow cells were then stained with IgD, IgM, CD19 and c-kit to discriminate the pro-B cell population (IgD⁻, IgM⁻, CD19⁺, c-kit⁺). Since all antibodies used for the pro-B cell staining were rat antibodies, env staining had to be performed in the absence of Fc-block and before the pro-B cell staining to avoid non-specific binding of the secondary α-rat Alexa-647.

Detection of Fc γ 2b was performed in the absence of Fc-block which would also recognize Fc γ 2b. Pro-B cells were stained with the same marker combination described above together with α -Fc γ 2b conjugated with PE-Cy7. After every incubation step, cells were washed with FACS buffer to remove the excess of antibody before analysis with FACS Canto.

DNA damage analysis - γ H2A.X foci enumeration

For γ H2A.X foci analysis, bone marrow cells were first labeled for B220-PE (eBiosciences) and then enriched by magnetic sorting using anti-PE MicroBeads (Miltenyi). Sorted cells were stained for CD19-APC (eBiosciences), fixed and permeabilized using a Foxp3 staining kit (eBioscience) according to the manufacturer's instructions. Subsequently, cells were incubated with rabbit anti-mouse phospho-histone H2A.X (Ser139) primary antibody (Cat# 2577, Cell Signaling) at the dilution of 1:1000 in blocking solution at 4°C overnight. Secondary antibody staining was performed with an Alexa Fluor 488-conjugated goat anti-rabbit IgG antibody diluted 1:1000 in blocking solution for 60 min at room temperature. DAPI was used to visualize nuclei.

A sample without primary antibody served as a negative control. For positive control, cells isolated from lethally irradiated mouse were subjected for the analysis as described above.

Images were captured from 100,000 cells at 60X magnification using the next generation imaging flow cytometry with the Amnis ImagestreamX Mark II (Millipore). The acquired data was analyzed with the IDEAS v6 software. γ H2A.X foci were enumerated using the spot count wizard according to the detailed protocol described before (Bourton et al., 2012; Parris et al., 2015).

Table S1. Regulated genes in *Setdb1*^{Mb1} pro-B cells.

[Click here to Download Tables S1](#)

Table S2. Expression of repetitive elements in *Setdb1*^{Mb1} pro-B cells.

[Click here to Download Tables S2](#)

Table S3. Expression of individual MLV elements in *Setdb1*^{Mb1} pro-B cells.

[Click here to Download Tables S3](#)

Table S4. Antibodies**FACS antibodies**

Reactivity	Clone	Fluorochrome	Provider
BP-1	6C3	PE	eBioscience
CD117	2B8	PE	Pharmin
CD11b (Mac-1)	M1/70	PE	Pharmin
CD11c	HL3	PE	Pharmin
CD127(IL7R α)	A7R34	PE-Cy5	eBioscience
CD16/32	93	PE-Cy7	eBioscience
CD19	1D3	PE	Pharmin
CD19	1D3	APC	Pharmin
CD19	1D3	APC-Cy7	Pharmin
CD24 (HSA)	M1/69	FITC	Pharmin
CD25	PC61	PE-Cy5	eBioscience
CD34	RAM34	Alexa-Fluor 647	eBioscience
CD34	RAM34	eFluor660	eBioscience
CD3e	145-2C11	PE	Pharmin
CD4	(L3T4)(PM4-5)	PE	Pharmin
CD43	S7	APC	Pharmin
CD45.1	A20	PE-Cy7	eBioscience
CD45.2	104	APC	eBioscience
CD45R (B220)	RA3-6B2	PE	Pharmin
CD45R (B220)	RA3-SB2	Alexa-Fluor750	eBioscience
CD5	53-7.3	PE	Pharmin
CD8a	53-6.7	PE	Pharmin
DX-5	DX5	PE	eBioscience
Env	82A25	N/A	Frank Malik
Fcblock(CD16/CD32)	2.4G2	N/A	Pharmin
IgD	11-26c.2a	FITC	Pharmin
IgM	II/41	FITC	Pharmin
Ly-6G (Gr-1)	RB6-8C5	PE	eBioscience
Rat IgG	polyclonal	Alexa647	Life Technologies
Sca-1	D7	FITC	Pharmin
Ter119	Ter-119	PE	eBioscience

ChIP antibodies

Epitope	Company	Catalog number	LOT	Technique
H3K9me3	Activ Motif	#39161.39162	#13509002	ChIP-qPCR
H3K4me3	Diagenode	#pAB-003-050	#A49-001	ChIP-qPCR
H3K4me3	Diagenode	#CS-003-100	A5051-001P	ChIP-qPCR
Setdb1	Santa Cruz	SC-66884X		ChIP-Seq
Setdb1	Thermo Scientific	PA5-30334		ChIP-seq
H3K9me3	Diagenode	pAb-056-050	A1675-001P	ChIP-Seq
H3K9ac	Millipore	#07-352	DAM1813175	ChIP-Seq

Table S5. Definition of hematopoietic cell types for FACS analysis and FACS sorting

Cell population	Gating strategy
Immature B	living cells, lymph, IgD-, B220+, IgM+
Mature B	living cells, lymph, IgM-, B220+, IgD+
pro-B	living cells, lymph, CD19+, IgD-, IgM-, c-kit+ CD25-
pre-B	living cells, lymph, CD19+, IgD-, IgM-, c-kit- CD25+
Fr. A	living cells, lymph, CD43+, B220+, HSA/CD24-/ low, BP-1-
Fr. B	living cells, lymph, CD43+, B220+, HSA/CD24+/high, BP-1-
Fr. C	living cells, lymph, CD43+, B220+, HSA/CD24 high, BP-1+
LSK	living cells, lin-, Sca+, c-kit+
CLP	living cells, lin-, IL7 α +, Sca low, c-kit low
CMP	living cells, lin-, IL7 α -, c-kit high, Sca-, CD34+, CD16/32-/ low
GMP	living cells, lin-, IL7 α -, c-kit high, Sca-, CD34+, CD16/32+
MEP	living cells, lin-, IL7 α -, c-kit high, Sca-, CD34-, CD16/32-
Pre-pro	living cells, lymph, lin-, IL7 α +, c-kit low, CD43low, B220+, CD93+
B cells	living cells, lymph, CD19+, B220+

Table S6. Primers for bisulfite PCR analysis

target	internal ID		sequence (5' to 3' direction)	taken from reference
IAP GAG region (478 bp)	GS2672	fw	aggtagtttggtgattggttttag	(Sadic et al., 2015)
	GS2673	rw	aatcaacaaaataaactccctaacc	
MLV group1 (256bp) (MLV4)	GS3758	fw	GTTTTTAAAATTTTTTAAAGATAAGATTAA	(Collins et al., 2015)
	GS3759	rw	TTATAATAAAATCTTTCATTCCCCC	
Emv2 (272 bp) (MLV8)	GS3764	fw	TTAGGGTTAGATTAGAGGGGTGGT	(Collins et al., 2015)
	GS3765	rw	CTAAATAACCCAATCAATAAATCC	

Table S7. Primer pairs for qRT-PCR and ChIP-qPCR analyses

Primer	Sequence	Experiment
MLV1-gag F	TCTTGGCCACCGTAGTTACAG	qRT-PCR/ChIP-qPCR
MLV1-gag R	CCAGTGTCCCTTTTCTTTGCAG	qRT-PCR/ChIP-qPCR
MLV5-gag F	AGCTCCAAAGAATCCGAAACG	qRT-PCR/ChIP-qPCR
MLV5-gag R	ATCTGTATCTGGCGGTTCCG	qRT-PCR/ChIP-qPCR
MLV8-gag F	TGACCCAGCGTCTCTTCTTG	qRT-PCR/ChIP-qPCR
MLV8-gag R	GGACCGCTTCTAAAAACATGGG	qRT-PCR/ChIP-qPCR
AI506816 F	CCTGCTATGAAGGGGACAAAG	qRT-PCR
AI506816 R	ATCTTCGGAAGAGCAGTCAGTG	qRT-PCR
Fcgr2b F	GGAAGGACACTGCACCAAGTC	qRT-PCR
Fcgr2b R	CCAGTGACAGCAGCCACAAT	qRT-PCR
Tubb3 F	GGCAACTATGTAGGGGACTCAG	qRT-PCR
Tubb3 R	ATGGTTCCAGGTTCCAAGTC	qRT-PCR
Gapdh F	TCAAGAAGGTGGTGAAGCAG	qRT-PCR
Gapdh R	GTTGAAGTCGCAGGAGACAA	qRT-PCR
Hprt F	ATGAGCGCAAGTTGAATCTG	qRT-PCR
Hprt R	CAGATGGCCACAGGACTAGA	qRT-PCR
Xbp1u F	GACTATGTGCACCTCTGCAG	qRT-PCR
Xbp1u R	CTGGGAGTTCCTCCAGACTA	qRT-PCR
Xbp1s F	GAGTCCGCAGCAGGTG	qRT-PCR
Xbp1s R	GTGTCAGAGTCCATGGGA	qRT-PCR
Hspa5 F	TGCAGCAGGACATCAAGTTC	qRT-PCR
Hspa5 R	TTCTGGGGCAAATGTCTTGG	qRT-PCR
Bcl2l11 F	GCTGTGTTCCACTTGATTCAC	qRT-PCR
Bcl2l11 R	AAGGTTGCTTGCCATTTGG	qRT-PCR
Pdia6 F	TGGTGGGTACAGTTCTGGAAAG	qRT-PCR
Pdia6 R	CACACCACGGAGCATAAACTC	qRT-PCR
IAPs-gag F	AGCAGGTGAAGCCACTG	ChIP-qPCR
IAPs-gag R	CTTGCCACACTTAGAGC	ChIP-qPCR
IAPs-global F	CGGGTCGCGGTAATAAAGGT	ChIP-qPCR

IAPs-global R	ACTCTCGTTCCCCAGCTGAA	ChIP-qPCR
Tubb3-intron1 F	TTCTGACTCGCATTCCCATCC	ChIP-qPCR
Tubb3-intron2 R	GGCTTAAGTGGCAACCTCAAAG	ChIP-qPCR
Def8-intron1 F	TGAGCCTTCGGTTTCACAAC	ChIP-qPCR
Def8-intron2 R	CAAAGCGCACCTCACATTTC	ChIP-qPCR
H19 F	AGCTTTGAGTACCCCAGGTTCA	ChIP-qPCR
H19 R	GCCTCTGCTTTTATGGCTATGG	ChIP-qPCR
Gapdh F	CCATCCCACGGCTCTGCAC	ChIP-qPCR
Gapdh R	GCAAGGCTTCGTGCTCTCG	ChIP-qPCR

Table S8. Plasmids

ID	plasmid name	fragments	cloning primers fw (5' to 3') or fragments	cloning primers rw (5' to 3') or fragments	origin	comment and usage
183	psPAX2	-	-	-	Didier Trono (Addgene: 12260)	Used for lentiviral packaging Fig. 7C, 7D
655	pLKO2mod/EGFP-WPRE	-	-	-	(Kuhn et al., 2010)	Used for GFP over-expression Fig. 7D
802	pLKO1mod	-	-	-	(Kuhn et al., 2010)	shRNA cloning Fig. 7C
811	pLP-eco-env	-	-	-	(Dambacher et al., 2012)	Used for lentiviral packaging Fig. 7C, 7D
849	pLKO1mod/shSCRAMBLED	-	-	-	(Dambacher et al., 2012)	Used for knockdown control Fig. 7C
963	pLenti6/EF1a-3FLAG-IRES-PURO	-	-	-	(Sadic et al., 2015)	Used as backbone for env overexpression Fig. 7D
1483	pLKO1mod/shBcl2l11-1	annealed oligos	CGCGTCCGGG ACGAGTTCAA CGAAACTTAC CTCGAGGTAA GTTTCGTTGAA CTCGTCTTTT GGAAA	CCGGTTTCCA AAAAGACGA GTTCAACGAA ACTTACCTCG AGGTAAGTTT CGTTGAATC GTCCCGGA	shRNA TRCN0000231244 (RNAi Consortium)	Used for knockdown of Bcl2l11 Fig. 7C
		backbone	XhoI	SpeI	pLKO1mod(#802)	
1502	pLenti6/EF1a-env1	env chr1 (CDS + genomic region downstream)	AGGTGTCGTG ACTAGTTTGGA TCCCACCATGG AAGGTCCAGC GTTCT	ACCAAGAACA AACCCAGCT	Pre-amplification from genomic DNA of wild type (C57Bl6/J) pro B cells	Used for env over-expression Fig. 7D
		env1 chr1 (CDS)	AGGTGTCGTG ACTAGTTTGGA TCCCACCATGG AAGGTCCAGC GTTCT	GTAATCCAGA GGTTGATTGA ATTCTATTCA CGCGATTCTA CTTCT	Amplification from gel-purified pre-amplification	
		backbone	BamHI digest	EcoRI digest	pLenti6/EF1a-3FLAG-IRES-PURO (#963)	

Supplementary references

- Beissbarth, T. and Speed, T. P.** (2004). GStat: find statistically overrepresented Gene Ontologies within a group of genes. *Bioinformatics* **20**, 1464-1465.
- Bock, C., Reither, S., Mikeska, T., Paulsen, M., Walter, J. and Lengauer, T.** (2005). BiQ Analyzer: visualization and quality control for DNA methylation data from bisulfite sequencing. *Bioinformatics* **21**, 4067-4068.
- Bourton, E. C., Plowman, P. N., Zahir, S. A., Senguloglu, G. U., Serrai, H., Bottley, G. and Parris, C. N.** (2012). Multispectral imaging flow cytometry reveals distinct frequencies of gamma-H2AX foci induction in DNA double strand break repair defective human cell lines. *Cytometry A* **81**, 130-137.
- Collins, P. L., Kyle, K. E., Egawa, T., Shinkai, Y. and Oltz, E. M.** (2015). The histone methyltransferase SETDB1 represses endogenous and exogenous retroviruses in B lymphocytes. *Proceedings of the National Academy of Sciences of the United States of America* **112**, 8367-8372.
- Dambacher, S., Deng, W., Hahn, M., Sadic, D., Frohlich, J., Nuber, A., Hoischen, C., Diekmann, S., Leonhardt, H. and Schotta, G.** (2012). CENP-C facilitates the recruitment of M18BP1 to centromeric chromatin. *Nucleus* **3**, 101-110.
- de Hoon, M. J., Imoto, S., Nolan, J. and Miyano, S.** (2004). Open source clustering software. *Bioinformatics* **20**, 1453-1454.
- Feng, X., Grossman, R. and Stein, L.** (2011). PeakRanger: a cloud-enabled peak caller for ChIP-seq data. *BMC bioinformatics* **12**, 139.
- Fuxa, M., Skok, J., Souabni, A., Salvagiotto, G., Roldan, E. and Busslinger, M.** (2004). Pax5 induces V-to-DJ rearrangements and locus contraction of the immunoglobulin heavy-chain gene. *Genes & development* **18**, 411-422.
- Heinz, S., Benner, C., Spann, N., Bertolino, E., Lin, Y. C., Laslo, P., Cheng, J. X., Murre, C., Singh, H. and Glass, C. K.** (2010). Simple combinations of lineage-determining transcription factors prime cis-regulatory elements required for macrophage and B cell identities. *Molecular cell* **38**, 576-589.
- Kim, D., Pertea, G., Trapnell, C., Pimentel, H., Kelley, R. and Salzberg, S. L.** (2013). TopHat2: accurate alignment of transcriptomes in the presence of insertions, deletions and gene fusions. *Genome biology* **14**, R36.
- Kuhn, P. H., Wang, H., Dislich, B., Colombo, A., Zeitschel, U., Ellwart, J. W., Kremmer, E., Rossner, S. and Lichtenthaler, S. F.** (2010). ADAM10 is the physiologically relevant, constitutive alpha-secretase of the amyloid precursor protein in primary neurons. *The EMBO journal* **29**, 3020-3032.
- Langmead, B., Trapnell, C., Pop, M. and Salzberg, S. L.** (2009). Ultrafast and memory-efficient alignment of short DNA sequences to the human genome. *Genome biology* **10**, R25.
- Mootha, V. K., Lindgren, C. M., Eriksson, K. F., Subramanian, A., Sihag, S., Lehar, J., Puigserver, P., Carlsson, E., Ridderstrale, M., Laurila, E., et al.** (2003). PGC-1alpha-responsive genes involved in oxidative phosphorylation are coordinately downregulated in human diabetes. *Nature genetics* **34**, 267-273.
- Parris, C. N., Adam Zahir, S., Al-Ali, H., Bourton, E. C., Plowman, C. and Plowman, P. N.** (2015). Enhanced gamma-H2AX DNA damage foci detection using multimagnification and extended depth of field in imaging flow cytometry. *Cytometry A* **87**, 717-723.
- Sadic, D., Schmidt, K., Groh, S., Kondofersky, I., Ellwart, J., Fuchs, C., Theis, F. J. and Schotta, G.** (2015). Atrx promotes heterochromatin formation at retrotransposons. *EMBO Rep* **16**, 836-850.
- Saldanha, A. J.** (2004). Java Treeview--extensible visualization of microarray data. *Bioinformatics* **20**, 3246-3248.

- Subramanian, A., Tamayo, P., Mootha, V. K., Mukherjee, S., Ebert, B. L., Gillette, M. A., Paulovich, A., Pomeroy, S. L., Golub, T. R., Lander, E. S., et al. (2005).** Gene set enrichment analysis: a knowledge-based approach for interpreting genome-wide expression profiles. *Proceedings of the National Academy of Sciences of the United States of America* **102**, 15545-15550.
- Trapnell, C., Hendrickson, D. G., Sauvageau, M., Goff, L., Rinn, J. L. and Pachter, L. (2013).** Differential analysis of gene regulation at transcript resolution with RNA-seq. *Nature biotechnology* **31**, 46-53.
- Zhang, Y., Liu, T., Meyer, C. A., Eeckhoute, J., Johnson, D. S., Bernstein, B. E., Nusbaum, C., Myers, R. M., Brown, M., Li, W., et al. (2008).** Model-based analysis of ChIP-Seq (MACS). *Genome biology* **9**, R137.

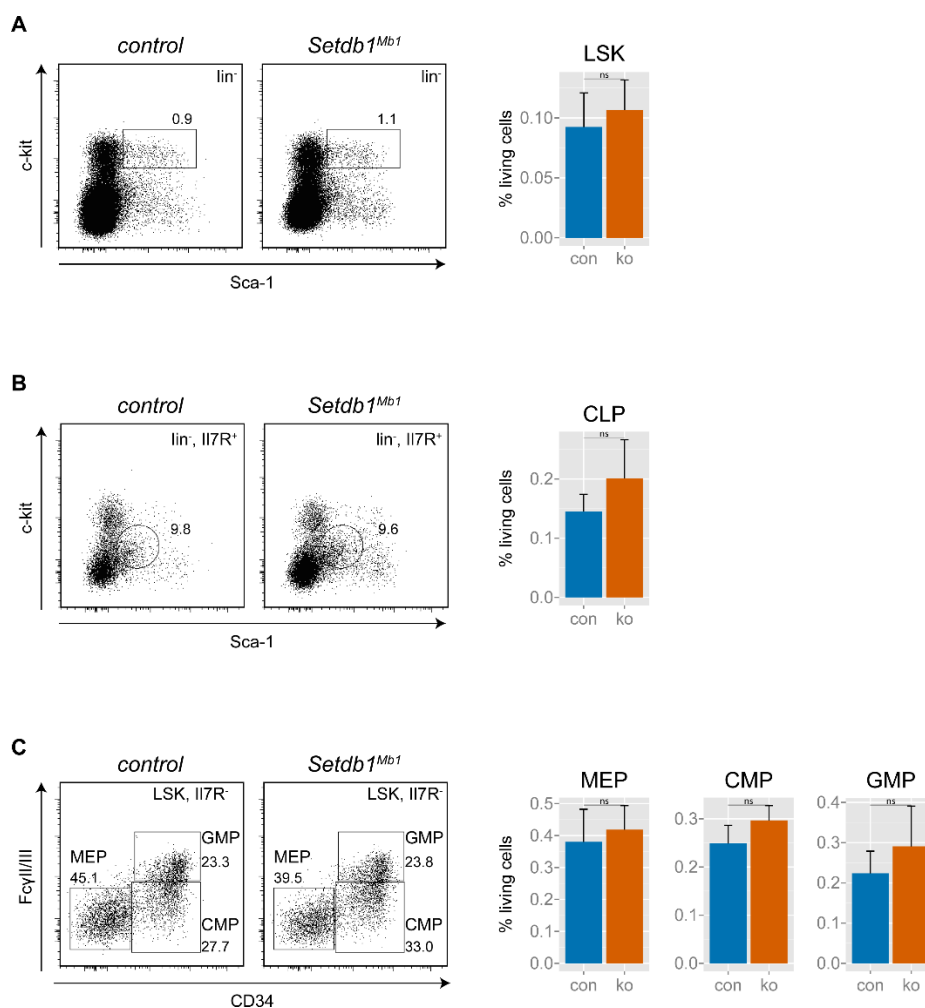


Figure S1. Normal frequencies of hematopoietic progenitors in *Setdb1^{Mb1}* mice

(A) FACS analyses of LSK cells (Lin⁻ Sca⁺ Kit⁺) in *control* (con) and *Setdb1^{Mb1}* (ko) bone marrow. Bargraph depicts average cell numbers as percentage of living cells from 6 mice per genotype. NS, not significant (unpaired two-tailed Student's t-test).

(B) FACS analyses of CLPs (Lin⁻ IL7Rα⁺ Sca^{low} Kit^{low}) in *control* (con) and *Setdb1^{Mb1}* (ko) bone marrow. Bargraph depicts average cell numbers as percentage of living cells from 6 mice per genotype. NS, not significant (unpaired two-tailed Student's t-test).

(C) FACS analyses of myeloid progenitors: CMPs (Lin⁻ IL7Rα⁻ Kit^{high} Sca⁻ CD34⁺ and CD16/32⁻); GMPs (Lin⁻ IL7Rα⁻ Kit^{high} Sca⁻ CD34⁺ and CD16/32⁺) and MEPs (Lin⁻ IL7Rα⁻ Kit^{high} Sca⁻ CD34⁻ and CD16/32⁻) in *control* (con) and *Setdb1^{Mb1}* (ko) bone marrow. Bargraph depicts average cell numbers as percentage of living cells from 6 mice per genotype. NS, not significant (unpaired two-tailed Student's t-test).

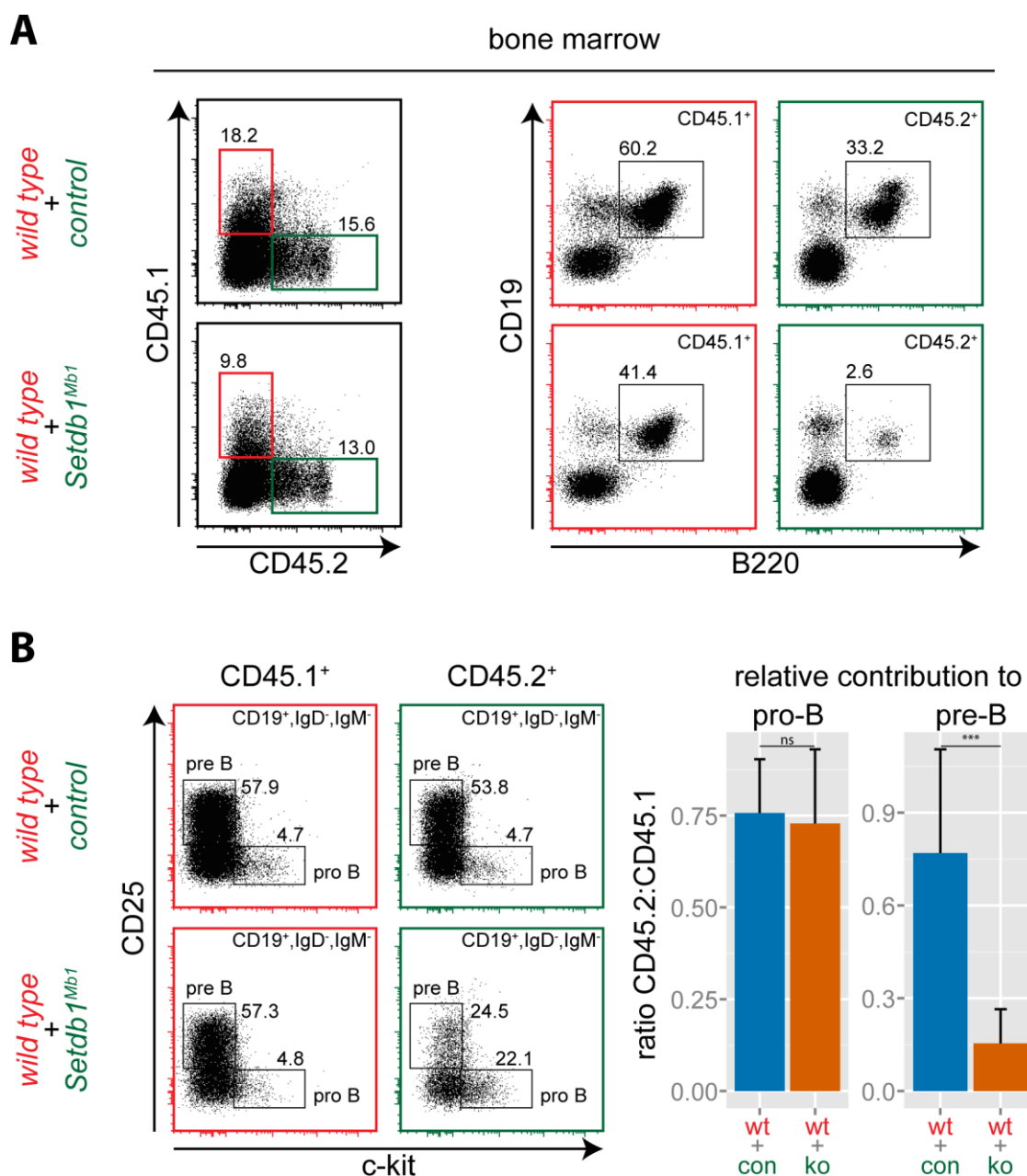


Figure S2. *Setdb1* has cell-intrinsic functions for B cell development.

(A) Representative FACS plots showing the relative contribution to the B cell lineage (B220⁺ CD19⁺) of wild type vs. *control* or *Setdb1*^{Mb1} donor bone marrow.

(B) Representative FACS plots showing contribution of donor bone marrow (wild type and *control* or wild type and *Setdb1*^{Mb1}) to pro-B and pre-B cell populations in recipient mice. Bargraph shows the quantification (n=3) of pro-B and pre-B cells in recipient mice as ratio between *control* (con) or *Setdb1*^{Mb1} (ko) to wild type (wt). ***P < 0.001 (unpaired two-tailed Student's t-test).

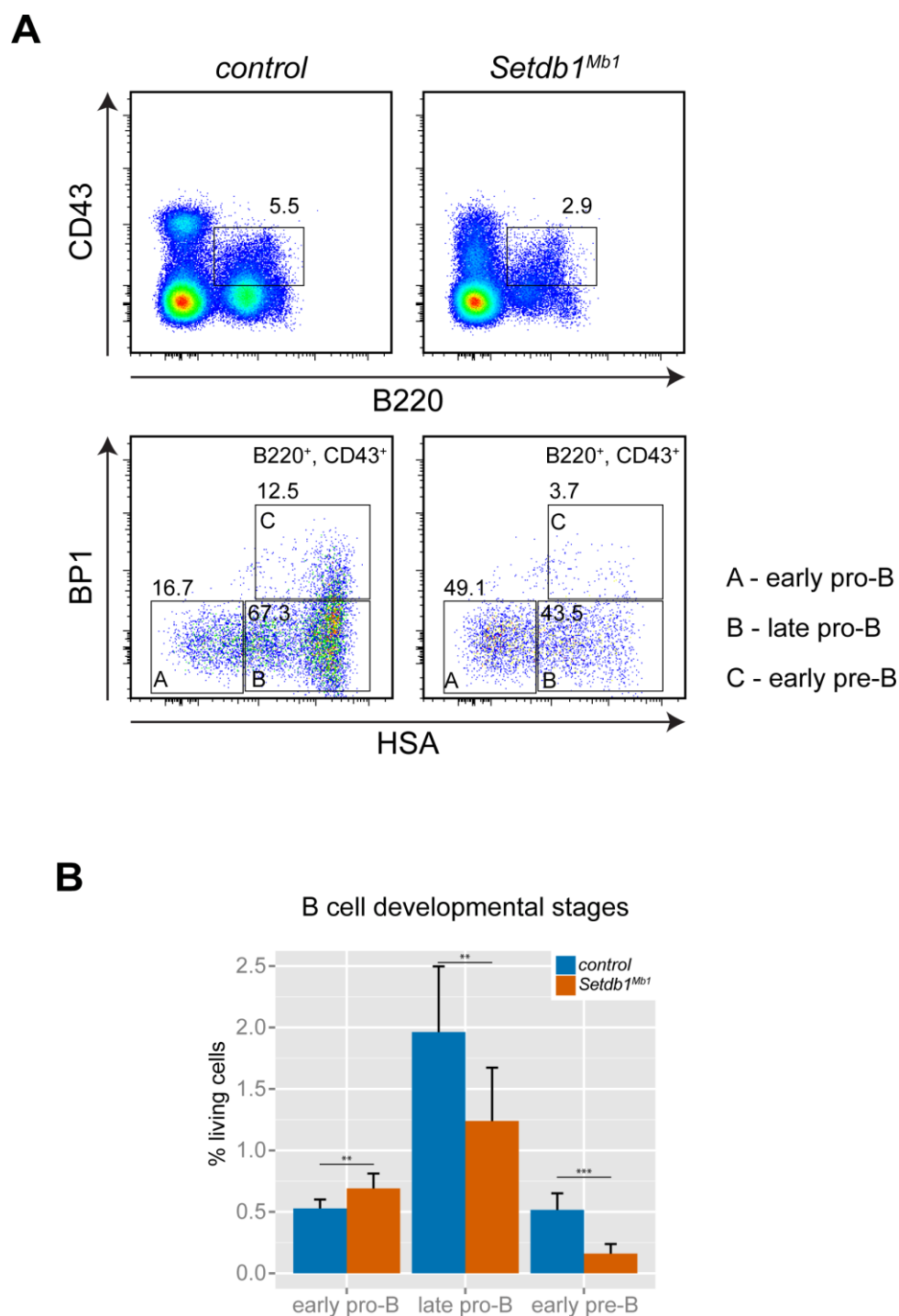


Figure S3. Block in pro-B to pre-B cell transition in *Setdb1^{Mb1}* mice.

(A) Distinct stages of B cell development were determined by FACS analysis of *control* and *Setdb1^{Mb1}* bone marrow according to Hardy, 1991: Fr.A (B220⁺ CD43⁺ HSA^{low} BP-1⁻), Fr.B (B220⁺ CD43⁺ HSA^{high} BP-1⁻) and Fr.C (B220⁺ CD43⁺ HSA^{high} BP-1⁺).

(B) Bargraph depicts average cell numbers of Hardy cell stages as percentage of living cells from 6 mice per genotype. ***P < 0.001, **P < 0.01 (unpaired two-tailed Student's t-test).

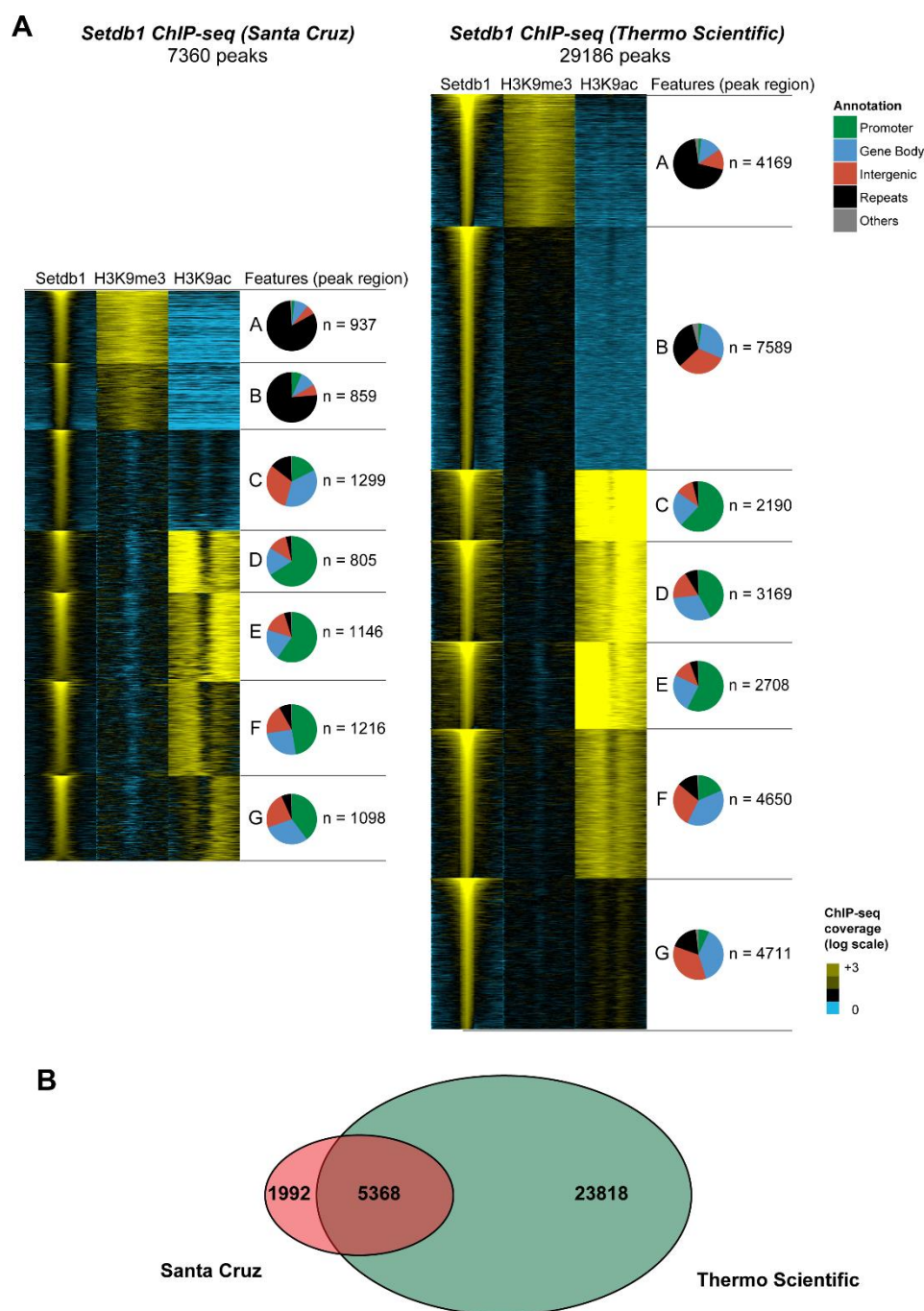


Figure S4. Comparative analysis of two independent *Setdb1* ChIP-seq datasets.

(A) ChIP-Seq analysis for *Setdb1* (Santa Cruz antibody and Thermo Scientific antibody), H3K9me3 and H3K9ac in short-term cultured *Rag2*^{-/-} pro-B cells. Heatmaps shows log-transformed read coverage for *Setdb1* and H3K9 modifications 1500 bp across all *Setdb1* binding sites identified in each dataset. Peak clusters were generated based on H3K9me3/H3K9ac occupancy using Cluster3 software. Pie charts depict the frequency of genomic features at *Setdb1* peaks in each cluster.

(B) Venn diagram depicting overlap between *Setdb1* peaks identified in the Santa Cruz vs. Thermo Scientific dataset.

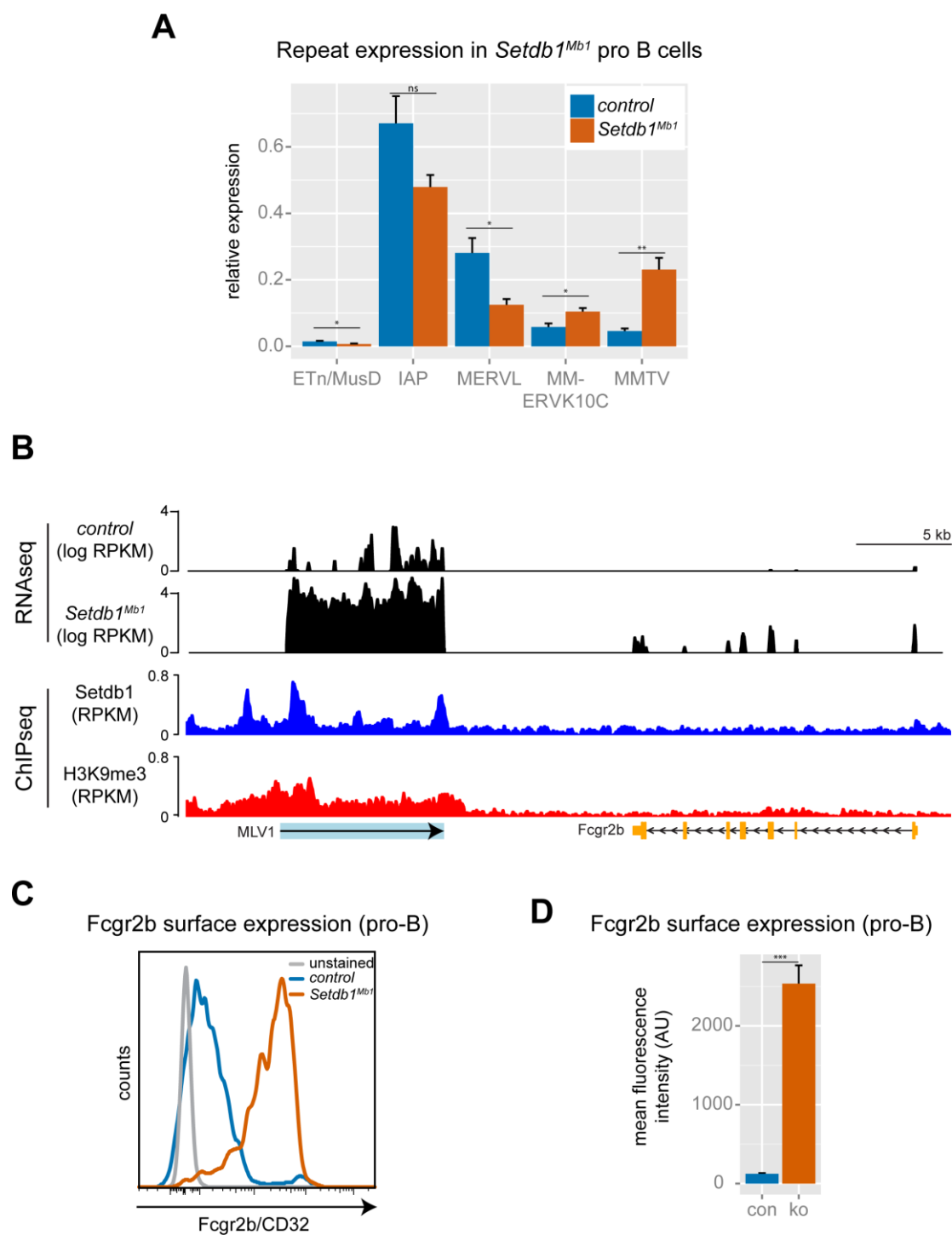


Figure S5. Retrotransposon expression; derepression of MLV1 and upregulation of Fcgr2b.

(A) Quantitative RT-PCR of retrotransposon classes in control vs. *Setdb1*^{Mb1} pro-B cells. Expression was calculated as relative expression to housekeeping genes from 6 biological replicates. NS, not significant; *P < 0.05 and **P < 0.01 (unpaired two-tailed Student's t-test).

(B) Coverage plot of normalized RNA-seq (control vs. *Setdb1*^{Mb1} pro-B cells) and ChIP-seq (short-term cultured *Rag2*^{-/-} pro-B cells) coverage across the genomic region of MLV1.

(C) Fcgr2b protein expression detected by FACS on control and *Setdb1*^{Mb1} pro-B cells (CD19⁺ IgM⁻ IgD⁻ CD25⁻ Kit⁺).

(D) Bargraph depicts the average Fcgr2b expression in *control* (con) and *Setdb1*^{Mb1} (ko) pro-B cells calculated as mean fluorescence intensity (MFI) from 6 mice per genotype. ***P < 0.001 (unpaired two-tailed Student's t-test).

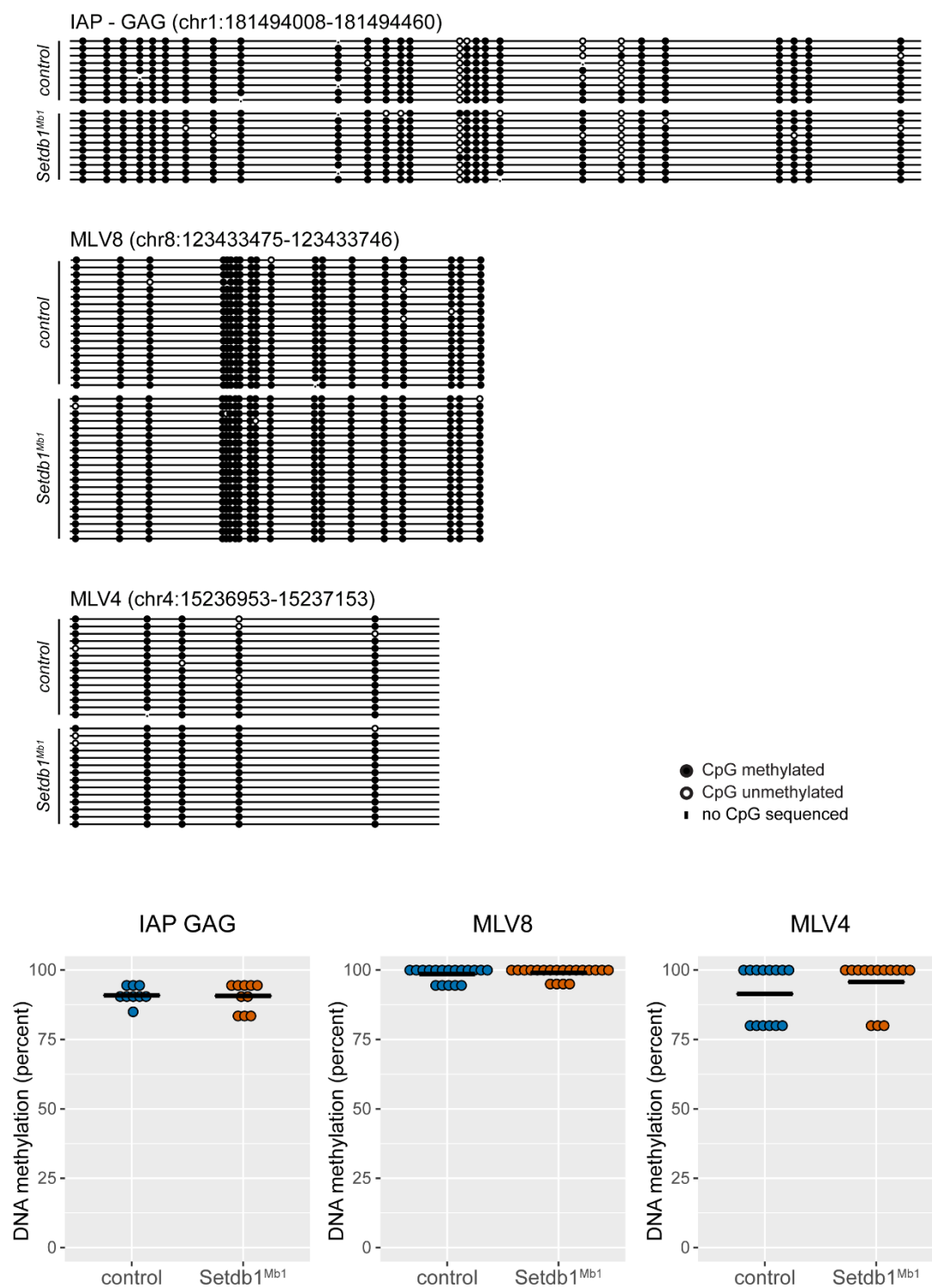


Figure S6. DNA methylation analysis of retrotransposons in pro-B cells.

DNA methylation of IAP GAG (no transcriptional change), MLV8 (derepressed) and MLV4 (no transcriptional change) was analyzed by bisulfite sequencing in control and *Setdb1*^{Mb1} pro-B cells.

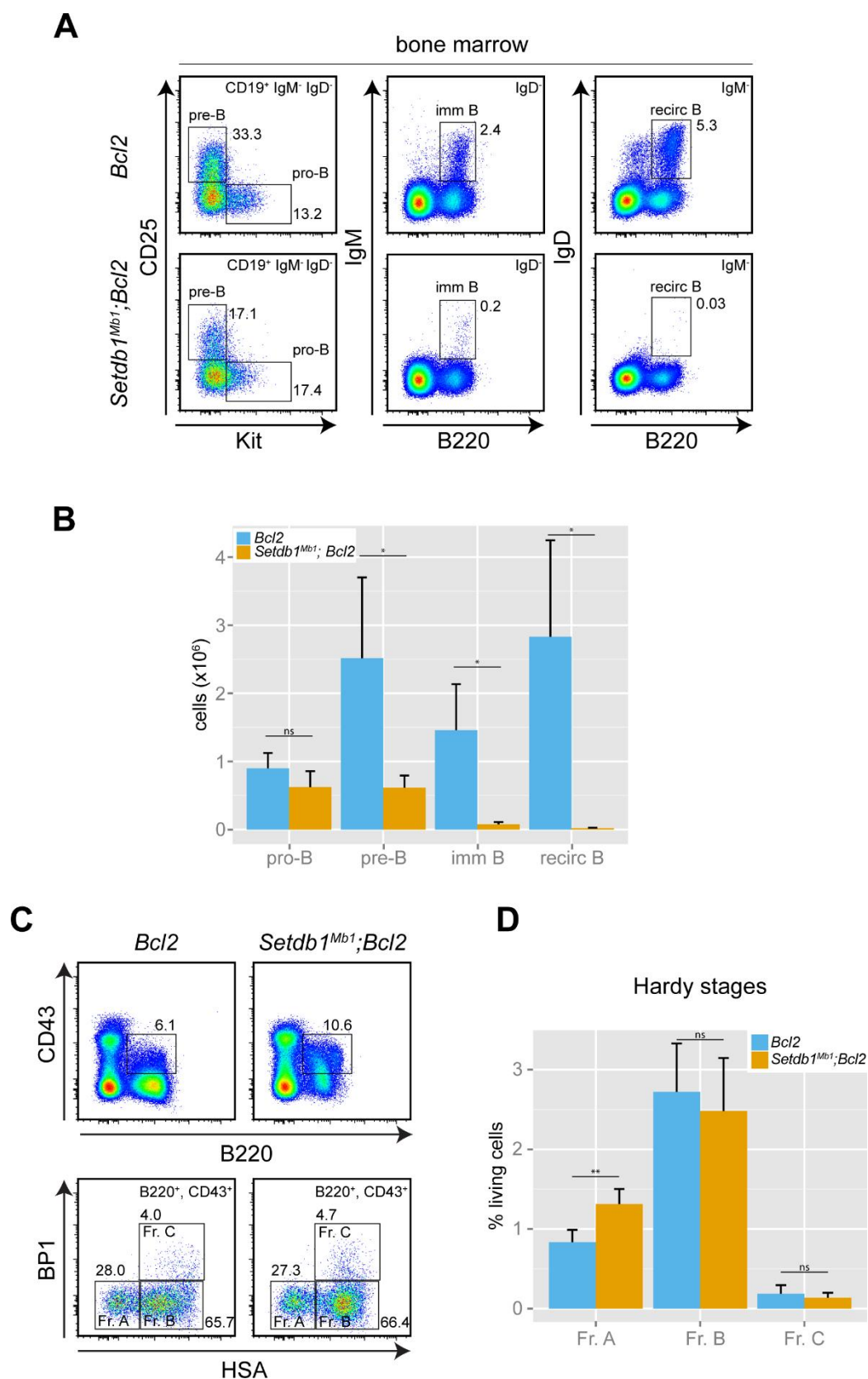


Figure S7. Forced expression of pro-survival Bcl2 partially rescues B cell development.

(A) Representative FACS plots showing different stages of B cell development in the bone marrow of *Bcl2* and *Setdb1^{Mb1}; Bcl2* mice.

(B) Bargraph showing average total cell numbers of B cell developmental stages in bone marrow from *Bcl2* and *Setdb1*^{Mb1}; *Bcl2* mice (n=6). NS, not significant; *P < 0.05, **P < 0.01 and ***P < 0.001 (unpaired two-tailed Student's t-test).

(C) Distinct stages of B cell development were determined by FACS analysis of *Bcl2* and *Setdb1*^{Mb1}; *Bcl2* bone marrow according to Hardy, 1991: Fr.A (B220⁺ CD43⁺ HSA^{low} BP-1⁻), Fr.B (B220⁺ CD43⁺ HSA^{high} BP-1⁻) and Fr.C (B220⁺ CD43⁺ HSA^{high} BP-1⁺).

(D) Bargraph depicts average cell numbers of Hardy cell stages as percentage of living cells from 6 mice per genotype. NS, not significant; **P < 0.01 (unpaired two-tailed Student's t-test).

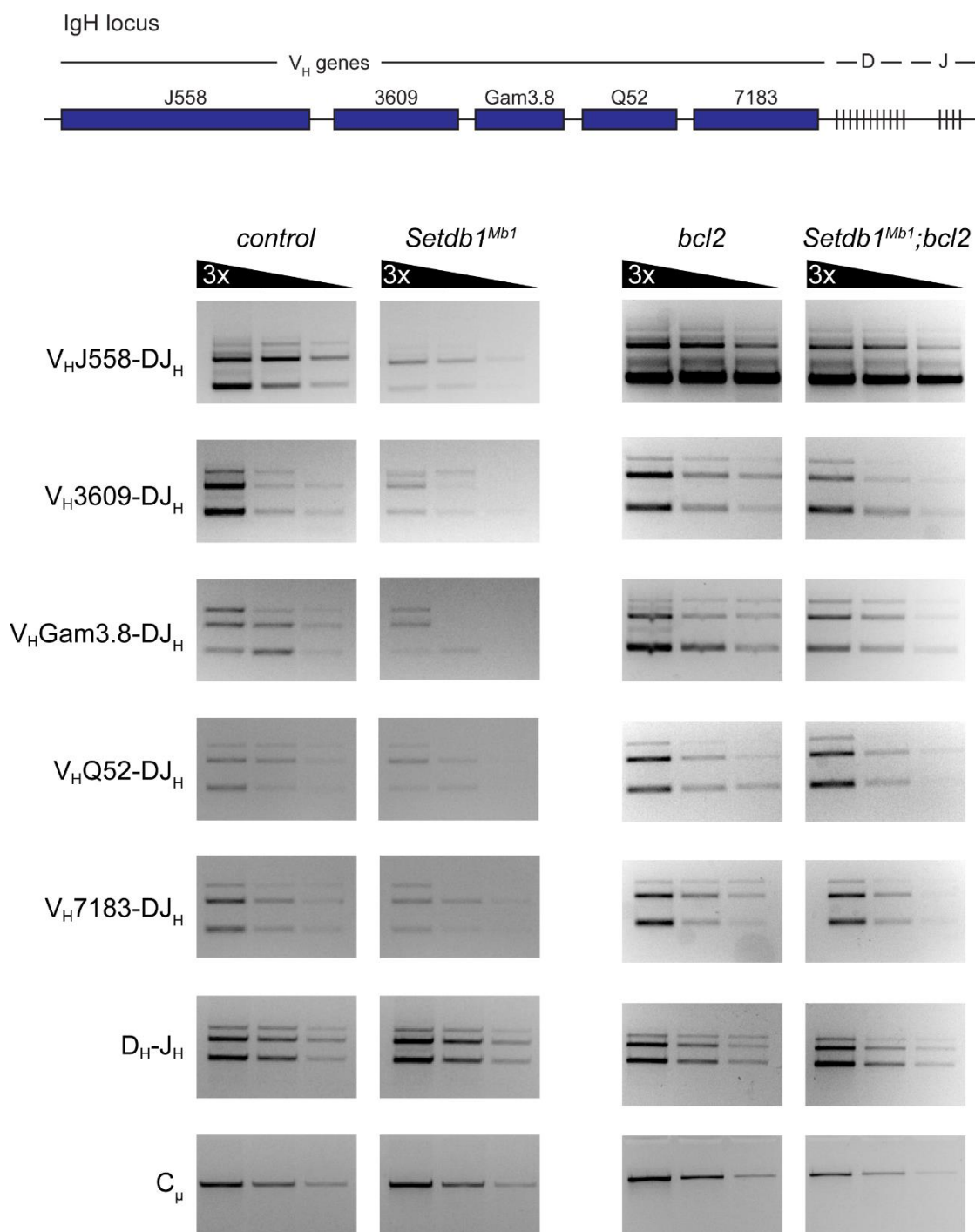


Figure S8. V-DJ recombination is not affected by loss of *Setdb1* in pro-B cells.

Schematic diagram of the V_H gene cluster of the *Igh* locus and the distal and proximal positions of the V_H gene families that were analyzed. DNA from control, *Setdb1*^{Mb1} as well as *Bcl2* and *Setdb1*^{Mb1}; *Bcl2* pro-B cells were analyzed for D_H-J_H and different V_H-DJ_H rearrangements by PCR of three-fold serial DNA dilutions. Input DNA was normalized by amplification of a PCR fragment from the IgH C_μ region.

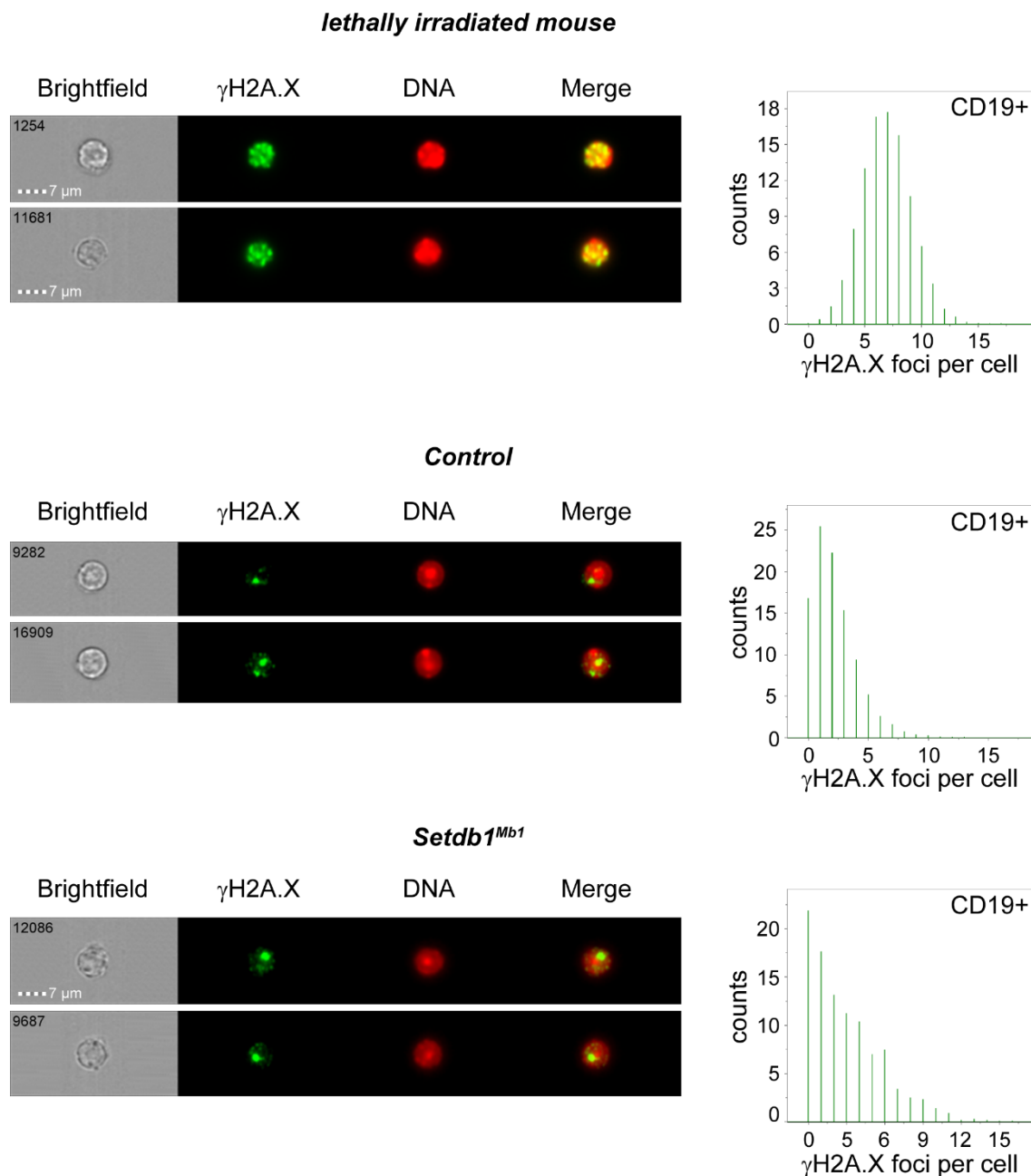


Figure S9. DNA damage analysis in B cells.

Representative images of CD19⁺ B cells stained with γ H2A.X antibody. Histograms show the distribution of foci number per cell. Cells from lethally irradiated mice show in average high numbers of γ H2A.X foci. Control and *Setdb1*^{Mb1} mutant cells display a comparable distribution of foci numbers per cell; the majority of cells show very few foci, which may stem from VD-J recombination events.

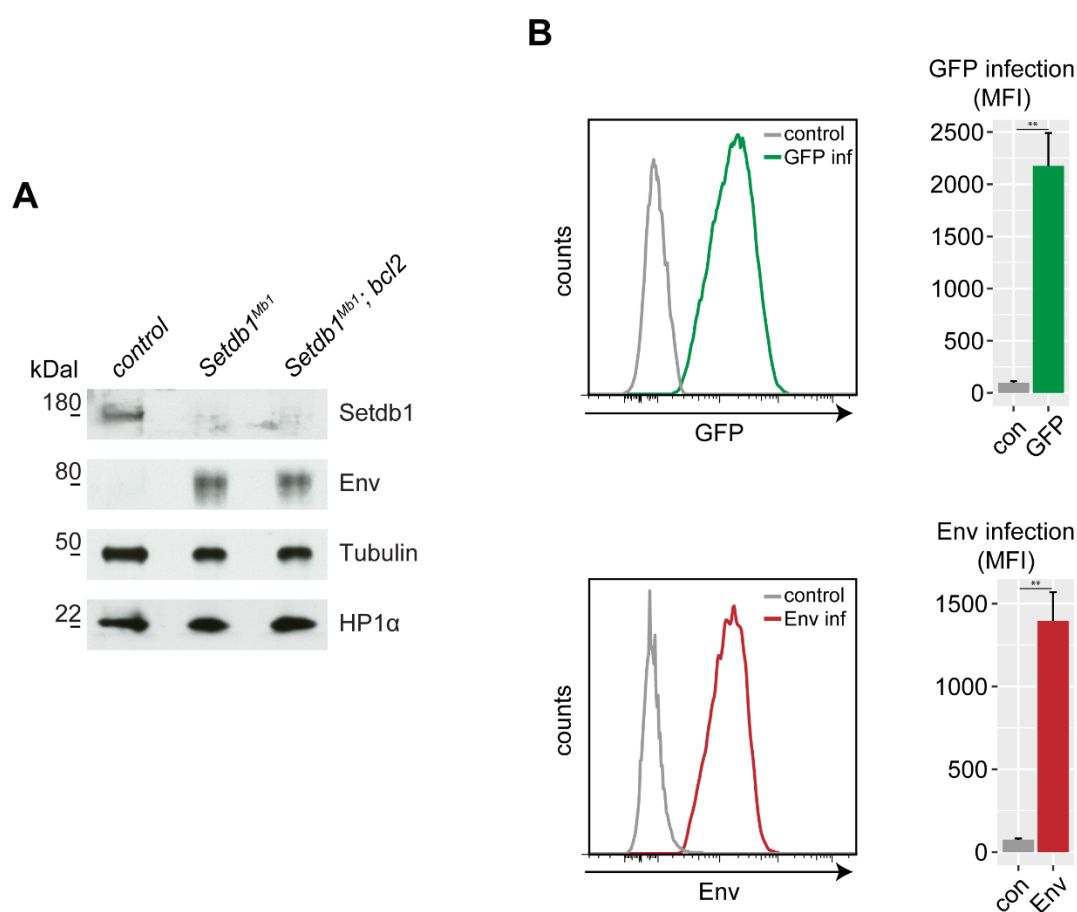


Figure S10. MLV Env overexpression in pro-B cells.

(A) Western blot analysis of sorted pro-B cells from control, *Setdb1^{Mbl}* and *Setdb1^{Mbl}; bcl2* mice. Both *Setdb1^{Mbl}* and *Setdb1^{Mbl}; bcl2* pro-B cells display loss of Setdb1 and strong expression of MLV Env protein. Tubulin and HP1 α serve as loading controls.

(B) Lineage negative bone marrow cells (control - non infected, GFP infected and MLV Env infected) were differentiated into B cells and expression levels of GFP and Env were measured by FACS analysis. Bargraphs depict the average GFP or Env expression calculated as mean fluorescence intensity (MFI) from 3 control vs. infected samples. **P < 0.01 (unpaired two-tailed Student's t-test).